

**EFFECT OF BAMBOO CHARCOAL ADDITIONS
ON SHEAR STRENGTH AND FRACTURE
BEHAVIOUR OF SN-BI SOLDER JOINT**

CHAI JING YEE

UNIVERSITI TUNKU ABDUL RAHMAN

**EFFECT OF BAMBOO CHARCOAL ADDITIONS
ON SHEAR STRENGTH AND FRACTURE BEHAVIOUR
OF SN-BI SOLDER JOINT**

CHAI JING YEE


**A project report submitted in partial fulfilment of the
requirements for the award of Bachelor of Materials and Manufacturing
Engineering with Honours**

**Lee Kong Chian Faculty of Engineering and Science
Universiti Tunku Abdul Rahman**

September 2024

DECLARATION

I hereby declare that this project report is based on my original work except for citations and quotations which have been duly acknowledged. I also declare that it has not been previously and concurrently submitted for any other degree or award at UTAR or other institutions.

Signature : 

Name : Chai Jing Yee

ID No. : 20UEB05658

Date : 9th SEPTEMBER 2024


APPROVAL FOR SUBMISSION

I certify that this project report entitled **“EFFECT OF BAMBOO CHARCOAL ADDITIONS ON SHEAR STRENGTH AND FRACTURE BEHAVIOUR OF SN-BI SOLDER JOINT”** was prepared by **CHAI JING YEE** has met the required standard for submission in partial fulfilment of the requirements for the award of Bachelor of Materials and Manufacturing Engineering with Honours at Universiti Tunku Abdul Rahman.

Approved by,

Signature

:



Supervisor

:

Dr Karen Wong

Date

:

7th October 2024

The copyright of this report belongs to the author under the terms of the copyright Act 1987 as qualified by Intellectual Property Policy of Universiti Tunku Abdul Rahman. Due acknowledgement shall always be made of the use of any material contained in, or derived from, this report.

© 2024, Chai Jing Yee. All right reserved.

ACKNOWLEDGEMENTS

I would like to thank everyone who had contributed to the successful completion of this project. I would like to express my gratitude to my research supervisor, Ts Dr Karen Wong Mee Chu for her invaluable advice, guidance and her enormous patience throughout the development of the research.

In addition, I would also like to express my gratitude to my loving parents and friends who had helped and given me encouragement in completing this report. Without them, I would not have resolved the problems I faced during my research work and report writing.

Last but not least, I would like to extend my gratitude to the UTAR administration for providing me with the essential laboratory facilities and instruments required to conduct extensive experiments. My deepest gratitude also goes out to the entire UTAR lab staff for all of the technical assistance they provided, which greatly improved the quality of my research.

ABSTRACT

Sn-Bi solders are considered by PV manufacturers as acceptable Pb-free alternative due to its low operating temperature and cost, despite being prone to brittleness caused by coarse Bi phases. Bamboo charcoal (BC) is a sustainable and environment-friendly resource with large surface area and its addition to Sn-Bi solder creates a green solder that complies with environmental regulations. This study contributed to the development of a high-performance Sn-58Bi alloy, demonstrated BC's role in enhancing solder joint reliability, and offered a sustainable alternative to Pb-based solders. The purpose of this study was to improve the shear strength and reduce the brittleness of the Sn-Bi solder alloy by adding a sustainable reinforcement (BC) to produce a low-cost, low-temperature, safe, environmentally friendly, and sustainable reinforced solder. Sn-58Bi solder paste was reinforced with 0.25, 0.50, 0.75 and 1.00 wt.% of activated BC, respectively and tested under accelerated aging at 120 °C for 7 and 14 days. Shear strength of the as-reflowed solder joints increased by about 21.67 % with 1.00 wt.% activated BC was added as reinforcement in the as-reflowed condition, and the 14-day aged samples showed less degradation (31.14 %) compared to pure Sn-Bi solder (49.28 %). Fracture surfaces showed transitions from flat and smooth surface to elongated-dimple structures with the addition of activated BC. Prolonged accelerated aging increased cleavage presence, while increasing amounts of activated BC reduced facet numbers and void size, indicating successful suppression of Bi phase segregation. Furthermore, no Mode 3 failures (failure in the intermetallic compound (IMC) layer) occurred when the as-reflowed samples contained 0.50 wt.% or more of activated BC, and the 7- and 14-day heat-aged samples were free from Mode 3 failures when the activated BC composition was at 0.75 wt.% and above. From this study, the recommended composition for improved PV module performance was determined to be Sn-58Bi with 1.00 wt.% activated BC.

TABLE OF CONTENTS

DECLARATION		i
APPROVAL FOR SUBMISSION		ii
ACKNOWLEDGEMENTS		iv
ABSTRACT		v
TABLE OF CONTENTS		vi
LIST OF TABLES		viii
LIST OF FIGURES		ix
LIST OF SYMBOLS / ABBREVIATIONS		xii
LIST OF APPENDICES		xiv
CHAPTER		
1	INTRODUCTION	1
1.1	General Introduction	1
1.2	Importance of the Study	2
1.3	Problem Statement	3
1.4	Aim and Objectives	4
1.5	Scope and Limitation of the Study	4
1.6	Contribution of the Study	5
1.7	Outline of the Report	5
2	LITERATURE REVIEW	6
2.1	Introduction	6
2.2	Soldering	6
2.3	Printed Circuit Boards (PCBs)	7
2.4	Reflow Soldering	8
2.5	Solder Flux	11
2.6	Sn-Pb Solder Alloy	12
2.7	Sn-Bi Solder Alloy	13
2.8	Intermetallic Compounds (IMCs)	15
2.9	Activated Carbon (AC)	17

2.10	Bamboo Charcoal (BC)	18
2.11	Shear Strength	19
2.12	Fractography	21
2.13	Summary	24
3	METHODOLOGY AND WORK PLAN	25
3.1	Introduction	25
3.2	Sample Preparation	25
3.3	Specimen Preparation	26
3.4	Reflow Soldering and Accelerated Aging	26
3.5	Shear Testing	27
3.6	Microstructural Fracture Analysis	28
3.7	Summary	29
4	RESULTS AND DISCUSSION	30
4.1	Shear test	30
4.2	Fracture Mode	35
4.3	Fractography	40
4.4	Summary	51
5	CONCLUSIONS AND RECOMMENDATIONS	53
5.1	Conclusions	53
5.2	Recommendations for future work	54
	REFERENCES	56
	APPENDICES	67

LIST OF TABLES

Table 2.1:	Eutectic Temperatures of Binary Sn Solders (Abteu and Selvaduray, 2000)	13
Table 2.2:	Element Cost (Cheng, Huang and Pecht, 2017)	14
Table 2.3:	Alloying Elements in Sn-Bi alloy	20
Table 2.4:	Fracture Failure Modes	21
Table 2.5:	Alloying Elements that Induce Ductile Failure Mode in Solder Matrix	23
Table 4.1:	Intermetallic Morphology After Reflow and After 14 Days of Aging	33
Table 4.2:	Fracture Failure Modes	36
Table 4.3:	Types of Failure Modes Observed	38
Table 4.4:	Percentage of Failure Modes for Sn-58Bi Reinforced by Different Weight Percentages of Activated BC	38
Table 4.5:	Predominant Failure Modes of Sn-58Bi Reinforced by Different Weight Percentages of Activated BC	39
Table 4.6:	Morphological Features and Observations with Increasing Activated BC Addition	47

LIST OF FIGURES

Figure 2.1:	Surface Mounting Process (Koji, 2019)	7
Figure 2.2:	Layers of PCB (Chan, 2023)	8
Figure 2.3:	SMT Reflow Soldering Process (Tsai, 2005)	9
Figure 2.4:	Temperature Profile of Sn-Bi (Chen et al., 2023)	10
Figure 2.5:	Schematic of a Solder Joint: (a) 2D; (b) 3D (Mookam and Kanlayasiri, 2018)	12
Figure 2.6:	Sn-Bi Phase Diagram (Wang et al., 2017a)	15
Figure 2.7:	Surface Morphologies of Sn-58Bi/Cu (Zhang, Zou and Zhang, 2011)	16
Figure 2.8:	SEM Micrograph of cross-sectional view of interfacial IMC: (a) Sn-Cu-Ni; (b) Sn-Cu-Ni-1.0AC (Ramli et al., 2016)	18
Figure 2.9:	Fracture Surfaces at Different Magnification: (a and b) Sn-Bi Solder; (c and d) Sn-Bi solder with 0.50 wt.% Al ₂ O ₃ (Hu et al., 2015)	22
Figure 2.10:	Kirkendall Voids within Cu ₃ Sn IMC layer (Weinberg and Böhme, 2009)	24
Figure 3.1:	Sn-58Bi-xBC Composite Solder Samples Preparation	25
Figure 3.2:	Single Lap Shear Joint Specimen	26
Figure 3.3:	Reflow Profile for Sn-58Bi Solder Assembly (ChipQuik, 2024)	27
Figure 3.4:	Universal Testing Machine (Shimadzu Autograph AGS-X Series)	28
Figure 3.5:	Hitachi S-3200 N Scanning Electron Microscope (SEM)	28
Figure 3.6:	Flowchart of Methodology	29
Figure 4.1:	Shear Test Results for Sn-58Bi Alloy with Varying Amounts of Activated BC Content	31
Figure 4.2:	IMCs and Kirkendall Voids in 14-Day Accelerated Aging Samples with 0.25 wt.% Activated BC	35

Figure 4.3:	IMCs Thickness with Varying Amounts of Activated BC Content	35
Figure 4.4:	Failure Modes of Solder Joint	36
Figure 4.5:	Micrograph of Activated BC Nanoparticles	40
Figure 4.6:	Element of Activated BC	41
Figure 4.7:	Carbon content in different activated bamboo charcoal reinforced Sn-58Bi (as-reflowed condition)	41
Figure 4.8:	Fracture Surface of As-Reflowed Samples with 0.00 wt.% Activated BC	43
Figure 4.9:	Fracture Surface of As-Reflowed Samples with 0.50 wt.% Activated BC	43
Figure 4.10:	Fracture Surface of As-Reflowed Samples with 1.00 wt.% Activated BC	44
Figure 4.11:	Intergranular Fracture of As-Reflowed Samples with 0.00 wt.% Activated BC	44
Figure 4.12:	Fracture Surface of 7-Day Accelerated Aging Samples with 0.00 wt.% Activated BC	45
Figure 4.13:	Fracture Surface of 7-Day Accelerated Aging Samples with 0.50 wt.% Activated BC	45
Figure 4.14:	Fracture Surface of 7-Day Accelerated Aging Samples with 1.00 wt.% Activated BC	46
Figure 4.15:	Fracture Surface of 14-Day Accelerated Aging Samples with 0.00 wt.% Activated BC	46
Figure 4.16:	Fracture Surface of 14-Day Accelerated Aging Samples with 0.50 wt.% Activated BC	47
Figure 4.17:	Fracture Surface of 14-Day Accelerated Aging Samples with 1.00 wt.% Activated BC	47
Figure 4.18:	Carbon Content Elements in Dimples of As-Reflowed Samples with 0.25 wt.% Activated BC	48
Figure 4.19:	Carbon Content Elements in Dimples of As-Reflowed Samples with 0.50 wt.% Activated BC	49
Figure 4.20:	Carbon Content Elements in Dimples of As-Reflowed Samples with 0.75 wt.% Activated BC	49

Figure 4.21:	Carbon Content in Dimples of As-Reflowed Samples with 1.00 wt.% Activated BC	50
Figure 4.22:	Fine Bi Precipitate (Sn-58Bi + 1.00 wt.% Activated BC) in As-Reflowed Condition	50
Figure 4.23:	Fine Bi Precipitate (Sn-58Bi + 1.00 wt.% Activated BC) in 7-Day Accelerated Aging Condition	50
Figure 4.24:	Fine Bi Precipitate (Sn-58Bi + 1.00 wt.% Activated BC) in 14-Day Accelerated Aging Condition	51

LIST OF SYMBOLS / ABBREVIATIONS

°C	degree Celsius
wt. %	weight percentage(s)
s	second(s)
min	minute(s)
kg	kilogram(s)
g	gram(s)
mm	millimetre(s)
kV	kilovolt(s)
α	alpha
β	beta
PV	Photovoltaic
PCB	Printed Circuit Board
SMT	Surface Mounting Technology
IMC	Intermetallic Compound
BC	bamboo charcoal
AC	activated carbon
2D	two-dimensional
3D	three-dimensional
USD	United States dollar
SEM	Scanning Electron Microscope
EDX	Energy Dispersive X-ray
DSSC	dye-sensitized solar cell
ASTM	American Society for Testing and Materials
BSE	backscattered electron
Sn	Tin
Pb	Lead
Cu	Copper
Ag	Silver

Bi	Bismuth
Zn	Zinc
In	Indium
Ni	Nickel
Ti	Titanium
O	Oxygen
V	Vanadium
Mg	Magnesium
Y	Yttrium
Al	Aluminum
Au	Gold

LIST OF APPENDICES

Appendix A: Figure

67

CHAPTER 1

INTRODUCTION

1.1 General Introduction

Soldering is an inevitable approach for building circuitry when it involves the packaging of electronic elements. The act of soldering employs solder to both physically and electrically join electronic element terminals to corresponding ones on Printed Circuit Boards (PCBs). Downsizing, dense assembly, and enhanced functionality are the major advancements in electronics packaging as the age of big data facilitates the generalization of the Internet of Things (IoT) and Artificial Intelligence (AI) (Zhang et al., 2022). One of the most prevalent approaches for attaching smaller and greater quantities of electronic elements to miniature PCBs is Surface Mounting Technology (SMT). Almost all contemporary electronic devices, including photovoltaic modules (PV), laptops and smartphones, make use of SMT packaging in some way.

The solar industry has expanded rapidly and is expected to continue to rise due to increased energy demand amidst the transition towards net-zero. The increased installation of PV results in huge volume of PV waste as solar panels have limited lifespan of 25 - 30 years (Padoan, Altimari and Pagnanelli, 2019). It is estimated that there will be 60 - 78 million tonnes of PV waste by 2050 (Weckend, Wade and Heath, 2016). This waste includes alarmingly toxic lead (Pb), which poses new challenge as Pb-containing solders are used in the metallization and connections of the PV modules. Eutectic Tin-Lead (Sn-Pb) solders have been considered benchmarks in the solar industry due to their extraordinary features and lengthy usage histories. Outstanding solderability, reliability, and cost-effectiveness are the hallmarks of these solders (Cheng, Huang and Pecht, 2017).

Presently, restriction on the use of Pb is being discussed at different regulatory levels (Weaver, 2022). According to the Environmental Protection Agency (EPA) (2000), Pb and its byproducts rank among the top seventeen detrimental contaminants. Thus, Bismuth (Bi)-containing solders are considered by PV manufactures as Pb-free replacement due to its low operating temperature and low cost, albeit inferior properties, such as brittleness due to coarsened Bi-

phase (Beetz, 2020; Shang et al., 2024; Hu et al., 2024). It meets the requirement of a green solder, and its low operating temperature will not require complete overhaul of the existing manufacturing line. Research on Tin-Bismuth (Sn-Bi), the low-temperature alternative solder alloy is still ongoing (Hutchins, 2019). Common methods to improve performance of Bi-containing solders include addition of alloying elements (Gain and Zhang, 2016b; 2017; Silva et al., 2017; Hu et al., 2018; Liu and Tu, 2020), reinforcement (Zhang et al., 2023) and heat-treatments (Ma et al., 2021; Li et al., 2022).

Bamboo charcoal (BC) is produced by heating bamboo at temperatures between 800 - 1200°C. This carbonization process creates a material with an exceptionally high surface area-to-mass ratio, enabling it to attract and retain a diverse array of substances, including chemicals, radio waves, moisture, odours, and harmful materials. By varying the temperature of carbonization, this material can be transformed from insulator to semiconductor and even to conductor as the pore size increases (Isa et al., 2016). Addition of activated carbon (AC) to Tin-Copper-Nickel (Sn-Cu-Ni) solder resulted in thinner intermetallic (IMC) layer and increased shear strength of the solder joint (Ramli et al., 2016). Among alternative carbon-based materials like carbon nanotubes, activated carbon, and graphene, bamboo stands out as a readily available and renewable biomass resource. This is largely due to bamboo's rapid growth rate, with the capability of expanding by at least 60 cm daily, making it a cost-effective option (Chaturvedi et al., 2024). Due to the inherently large specific surface area and abundant pores, this environmentally friendly and sustainable plant-based reinforcement is expected to achieve maximum contact with the Bi-phase to suppress the coarsening and thus reduce brittleness.

In this study, the shear strength, failure modes and fracture behaviour of Sn-58Bi solder alloy reinforced by varying weight percentages (wt.%) of BC was investigated.

1.2 Importance of the Study

This study explores the viability of Pb-free Sn-Bi solder alloys as a substitute for conventional Sn-Pb solder alloys. In the solar industry, Sn-Bi solder alloys are a safer alternative to Pb, which is consistent with the current shift to Pb-free materials, given the toxicity of Pb to humans and the environment. Additionally,

their low melting point enables a reduced processing temperature, thereby offering cost savings in comparison to Sn-Pb alternatives. Sn-Bi exhibits less favorable mechanical characteristics than Sn-Pb. Nevertheless, the mechanical properties of Sn-Bi solder joints may be improved by incorporating BC into them. This approach could possibly increase their level of competitiveness when compared to Sn-Pb.

Shear studies are required to determine the reliability of these joints and assure their ability to endure mechanical stress. Important insights are gained from examining the effects of BC on the microstructure and failure behavior of Sn-Bi solder joint. Utilizing this data can lead to improved solder joint designs and fabrication processes, which in turn can result in better, more eco-friendly, and more reliable PV module assemblies.

If the technique of employing BC as reinforcement for Sn-Bi solder joints is successful, there are several possible advantages. BC originates from renewable resources, indicating that it promotes sustainable manufacturing practices and mitigates adverse ecological impacts. Its extensive availability and cost-effectiveness also make it a desirable choice for improving solder joint performance without increasing manufacturing expenses.

1.3 Problem Statement

Low-melting-point alloys for Pb-free soldering have gained popularity as a result of numerous nations' legislation limiting the usage of Sn-Pb solder in a variety of settings due to Pb's toxicity. Reliable joints necessitate solder with a low melting point, particularly when it comes to delicate electronic components that ought to be kept at lower temperatures to prevent damage. An optimal soldering temperature is essential to minimise mechanical or thermal stress on the solar cells and PCB. Eutectic Sn-Bi solder, which melts at 139 °C, is a potential substitute to Sn-Pb solder, which has a eutectic temperature of 183 °C (Yeh, Chang and Straumal, 2011). Thus, Bi-containing solders are the most suitable replacement candidate due to their lower soldering temperature compared to Pb solder, eliminating the need for new production line setups.

However, the brittleness of the coarse Bi-rich phase in irregular eutectic Sn-Bi solders could potentially compromise joint reliability and limit further application (Wang et al., 2015). Even so, the Pb industry has replaced

one-third of global Pb soldering with Bi solders, largely because of their lower cost (Weckend, Wade and Heath, 2016). Solder joints, which are critical for electrical and mechanical linkages, experience mechanical loads and strains when the solar cells and PCB exhibit variable thermal expansion rates while in operation. Solder's shear strength is dictated by its microstructure and IMCs layer development. Greater strength is achieved with finer microstructures and with thinner IMCs layer. Similar to AC, introducing BC as reinforcement to Sn-Bi solder may optimize its microstructure and suppress the IMCs layer growth. Thus, the problem statement of this study was to examine whether introducing BC to Sn-Bi solder alloys could improve their shear strength and fracture behavior.

1.4 Aim and Objectives

The aim of this study was to improve the shear strength and reduce the brittleness of the Sn-Bi solder alloy by adding a sustainable reinforcement (bamboo charcoal, BC). This aligns with the goal of using a low-cost, low-temperature, safe, and environmentally friendly alternative, making Sn-Bi the only candidate being considered by PV manufacturers. In pursuit of this aim, three objectives were defined:

- (i) To compare shear strength of Sn-Bi solder joints with BC reinforcement.
- (ii) To identify types of fracture in Sn-Bi solder joints with bamboo charcoal reinforcement.
- (iii) To elucidate the microstructure-fracture mode relationship due to addition of BC.

1.5 Scope and Limitation of the Study

This study focused on the impact of BC reinforcement on Sn-58Bi solder alloys. The reinforcement amounts range from 0.25 wt.% to 1.00 wt.%, with 0.25 wt.% increments, and the substrate employed was copper-based PCB. Reflow soldering was the selected soldering procedure, and mechanical shear tests were carried out on single-lap joints.

However, the experimental setups and conditions are simplified, and thus may not fully reflect the complications of actual soldering procedures in workplaces. Furthermore, there is no prior research to compare and validate the accuracy of the results obtained as this experiment has not been performed before. Consequently, this presents a challenge in evaluating the significance of the results and their practicality.

1.6 Contribution of the Study

The main purpose of this research is to create a high-performance, Pb-free Sn-58Bi solder alloy that provides a more reliable alternative to conventional Pb-based solder alloys. This research investigated the influence of BC reinforcement on the shear strength and fracture behaviour of Sn-58Bi solder joints, introducing novel approaches to improve their reliability and durability, particularly in applications that necessitate mechanical integrity under stress. Furthermore, the research emphasized BC as an innovative reinforcement material, thereby advocating for the implementation of sustainable alternatives in soldering, as bamboo is a renewable resource. This contribution is beneficial for industries that are striving to mitigate environmental impact and advance materials science and engineering.

1.7 Outline of the Report

The Final Year Project report is structured into five chapters, each of which addresses a specific subtopic. Chapter 1 introduces the report and addresses its path of action. Chapter 2 provides a detailed assessment of relevant subtopics in the present body of literature. Chapter 3 outlines the approaches that should be used to attain the intended outcomes. Chapter 4 analyses the effect of BC nanoparticle reinforcement on the Sn-58Bi solder joint. Chapter 5 provides a comprehensive summary of the whole project.

CHAPTER 2

LITERATURE REVIEW

2.1 Introduction

This section conveys valuable insight into soldering, outlining the techniques and components associated. It compares the standard lead-based solder, Sn-Pb, to the lead-free solder, Sn-Bi. Furthermore, it investigates the possible improvement of solder joints by incorporating BC into Sn-Bi alloys by analysing the shear strength and microstructural fracture mechanism of solder joints.

2.2 Soldering

Soldering involves the connection of two or more metallic parts using a fusible metallic alloy known as solder, which has a lower melting point than the metals being bonded (Kumar and Maurya, 2022). When solder is applied to the joint and heated to its melting point, it seeps into the space between the metal pieces and solidifies, establishing a bond. This melting process ensures that the solder thoroughly wets the components, promoting adhesion as it cools. Generally, an ideal solder joint is characterised by a smooth and glossy surface, and complete, solid wetting (Bara, 2020). Following the metal attachment, the solder joints fulfill several essential functions. By physically binding assemblies together, it secures their attachment and regulates the heat-induced fluctuation in movement of individual components. Apart from eliminating heat, it retains electrical current flowing smoothly across the joint, which is essential for constructing circuits (Aamir et al., 2020).

Soldering is a crucial process in electronics manufacturing that allows electronic components, especially those installed on PCB, to be mechanically and electrically connected (Zhong et al., 2022). Miniaturization and multi-functioning features are becoming more significant in electronic devices as the industry continues to grow at a rapid pace in response to the ever-increasing demands of consumers. This shift has prompted advancements in electronic packaging technology that aim to achieve greater integration, functionality, and density (Jiang et al., 2019). These days, surface-mounted components account

for almost 90 % of all commercial electronic devices, with through-hole components accounting for the negligible remainder (Illés, Krammer and Géczy, 2020)

A typical procedure in SMT is demonstrated in Figure 2.1. The three fundamental steps of this manufacturing procedure are solder printing, component positioning, and reflow soldering. Initially, solder is deposited onto the PCB. Above this solder material, the electronic components are subsequently positioned. In the process of reflow soldering, the assembled PCB is gradually heated in a reflow oven. Under these conditions, solder joints form between the PCB and the components, guaranteeing the electronic assembly's reliability and operation.

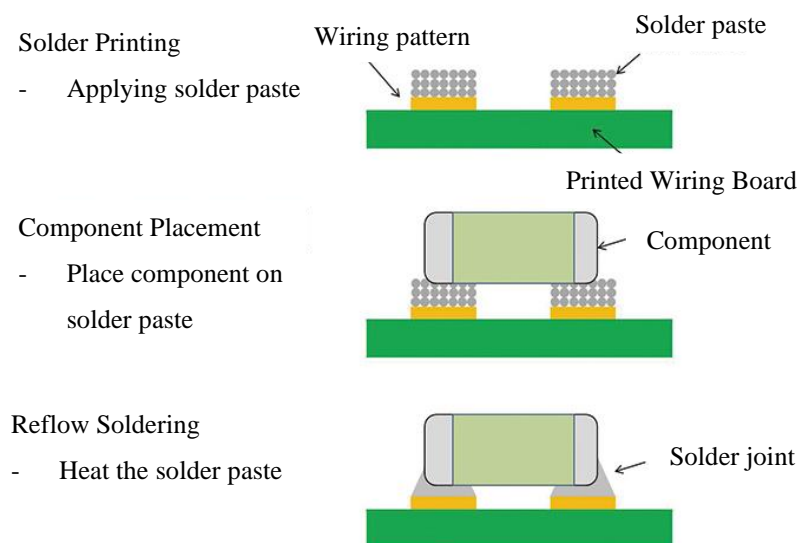


Figure 2.1: Surface Mounting Process (Koji, 2019)

2.3 Printed Circuit Boards (PCBs)

PCBs design and fabrication are now an independent discipline in electronics. A PCB is a necessary component for integrating electronic elements into a miniature final product, as it offers reliable support for the elements and permits electrical interactions between them. They also define the functionality and construction of an electronic device (Peterson, 2024). All PCBs adhere to a fundamental framework. The four essential layers consistently found on a PCB include the substrate, copper, solder mask, and silkscreen, as illustrated in Figure 2.2.

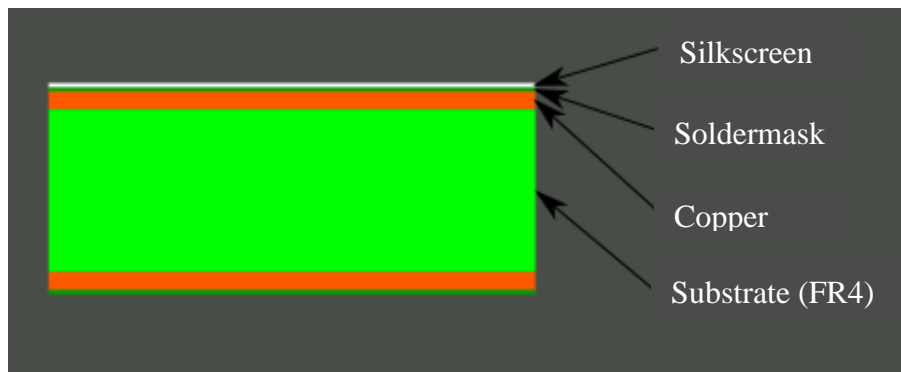


Figure 2.2: Layers of PCB (Chan, 2023)

Strength and thickness are imparted by the substrate material, which is commonly known as "FR4" fiberglass, which forms the sturdy base of the PCB. The board is subsequently coated with a thin film of copper foil that is adhered to it. Each type of PCB possesses distinct functionalities that are optimized by its specific number of copper layers. A PCB might have one layer, two layers, or multiple layers of copper foil. Furthermore, a standard PCB's characteristic green hue is caused by the solder mask layer, which is situated above the copper foil. By physically separating the copper traces from one another, this layer renders solder jumpers impossible and facilitates precise soldering. After that, the solder mask layer is coated with a white silkscreen. The components functionalities appear visually on the silk screen labels (Perdigones and Quero, 2022)

Research in this project focused on the phases present in the solder alloy interfacial layers with the Cu substrate of the PCB. For simplicity's sake, this project used blank PCBs with only exposed Cu surfaces, even though a complete PCB usually consists of multiple layers.

2.4 Reflow Soldering

Conventional procedures used in large-scale PCB manufacturing include wave soldering and reflow soldering, although alternative soldering methods are also employed. For this project, reflow soldering was selected because it uses solder paste efficiently, only needs to be applied where soldering is required, and is easy to monitor and regulate. This method is indispensable in the electronics sector, particularly for the mounting of surface-mount components to PCBs (Whalley, 2004).

Figure 2.3 illustrates reflow in relation to components that are surface-mounted. Reflow soldering is comprised of three fundamental steps. Initially, solder paste is applied to specific apertures of the PCB by pushing a squeegee through the stencil. The components are subsequently introduced via automatic placement devices onto the deposited solder paste. Following that, the solder paste is melted and reflowed in the oven for assembly purpose. The desired mechanical and electrical attachments between the PCB and electronic components will be established once the assembly has cooled and the solder material has solidified (Illés, Krammer and Géczy, 2020).

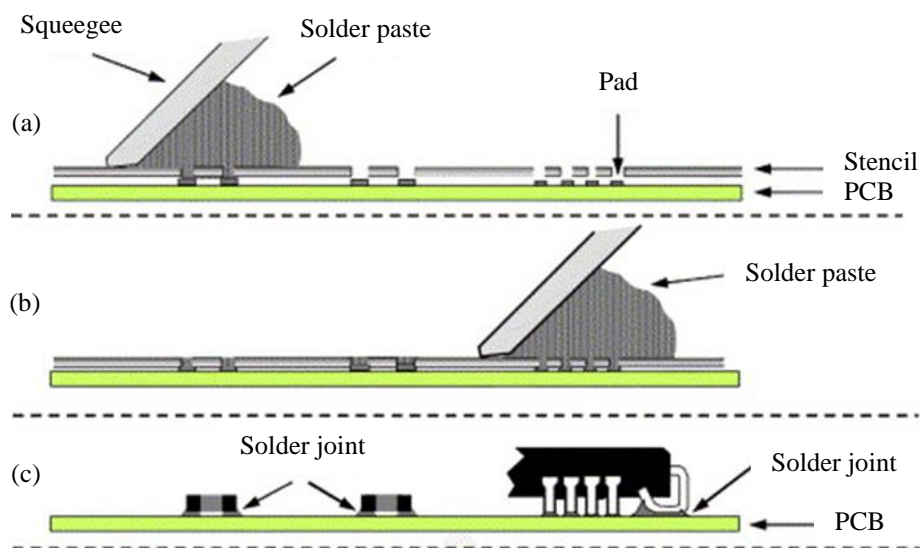


Figure 2.3: SMT Reflow Soldering Process (Tsai, 2005)

The solder generally adheres to a certain temperature profile during a reflow operation in the furnace. This profile is frequently illustrated with time-temperature graphs, and it is heavily influenced by the flux and solder employed. Solder specifies the appropriate temperature range, whereas flux determines the reflow conditions (Siti Rabiattull Aisha et al., 2015). Manufacturers frequently issue approximate profiles that are specific to their compositions. The three primary stages of the reflow operation are preheating, reflowing, and cooling, as illustrated in Figure 2.4.

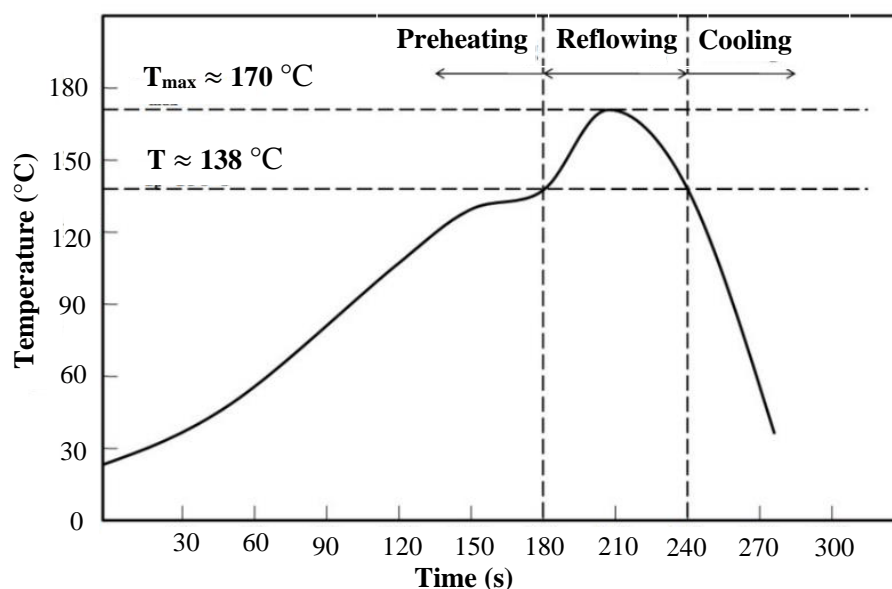


Figure 2.4: Temperature Profile of Sn-Bi (Chen et al., 2023)

Preheating is the process of shielding components from thermal stress and degradation by gradually increasing the furnace temperature of the PCB assembly. The biggest concern at this point is temperature acceleration: abrupt heating could distort components, whereas gradual heating could hasten the solder paste's evaporation. Thus, it is recommended to preheat the assembly to approximately 80 °C to 110 °C at a rate of 3 °C/s (Siti Rabiattull Aisha et al., 2015; Chen et al., 2023)

During the soaking phase, the primary goal is to maintain a consistent temperature throughout the PCB. This facilitates activating the flux in the solder paste and eliminating any oxides from the soldering surfaces. In some manufacturing configurations, the preheating and thermal soak phases might be considered one and the same, with the designation "preheat" applied to both. But even in these instances, the onset and end of the phase exhibit different rates of temperature increase. The soaking phase temperature will reach the solder alloy's liquidus onset temperature, which varies from 138 °C to 139 °C in the case of Sn-Bi solder alloy and maintain for 1 to 2 minutes (Siti Rabiattull Aisha et al., 2015; Chen et al., 2023; Waseem, 2023).

During the reflow phase, the Sn-Bi solder paste liquefies, establishing a robust metallic connection between the parts and the PCB as the temperature inside the furnace surpasses the solder paste's melting point. Reflow causes a

significant increase in temperature throughout the assembly to ensure optimal wetting by lowering the viscosity of the solder paste. The typical reflow temperature of Sn-Bi solder is found to range from 138 °C to 170 °C at a rate of 8 °C/s (Siti Rabiattull Aisha et al., 2015; Chen et al., 2023; Palaniappan and Martin, 2016).

During the cooling phase, the solder joints undergo an abrupt reduction in temperature, solidifying at a rate ranging between 20 °C/s and 30 °C/s, resulting in the intended formation of a fine-grained microstructure (Siti Rabiattull Aisha et al., 2015). It is essential for the assembly to reach a temperature below the solder liquidus level before being withdrawn from the oven to mitigate the detachment of the assembled components.

2.5 Solder Flux

Solder paste comprises of flux paste integrated into solder powder, which attaches components together until the solder disintegrates during the reflow soldering operation. The standard metal-to-flux ratio in solder paste is 45:55 by volume (Kaya, 2019). There are three fundamental kinds of soldering flux: organic, inorganic and rosin. Organic flux exhibits a significant fluxing reaction. A deionized water rinse is an effective method of eliminating the corrosive properties of the substance subsequent to its application. In addition, inorganic flux is frequently employed in applications involving more durable metals such as brass, stainless steel, and various others. Its strong and aggressive character makes it unsuitable for use in electronic devices, where any residue could harm solder connections. Rosin flux is an exceedingly prevalent and extensively utilized flux variety, especially in electronic settings. Its secure and desirable innocuous residual that it imparts to assemblies is particularly advantageous (Dušek and Náhlík, 2012; Liu, Xue and Liu, 2018). This project makes use of rosin flux.

Rosin flux serves a multitude of functions within the realm of soldering. By undergoing heating, the substance effectively eliminates impurities and oxides from metal surfaces, thus fulfilling its function as a cleaning agent (Zuberbuehler, 2021; Dušek et al., 2021). This ensures a flawless surface condition that facilitates soldering, consequently enhancing adherence and solder joint integrity. Furthermore, rosin flux enhances the wettability of the

solder, which enables the application of a consistent stream of molten solder by lowering surface tension, ensuring reliable connections (Dušek et al., 2021). Figure 2.5 is a schematic depiction of a solder joint. As the contact angle decreases, the wettability improves as a good wettability feature eliminates the possibility of insufficient coverage or gaps. The ideal contact angle is below 40 degrees (Zhai et al., 2021). Moreover, rosin flux serves as a defensive barrier, hindering the formation of oxides on metallic surfaces throughout the soldering procedure. The effectiveness of this protective layer in obstructing airborne particles from reaching the purified metal facilitates the establishment of a sound solder joint (Görlich et al., 2010).

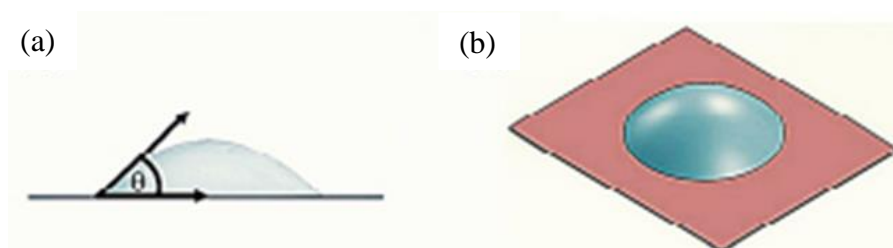


Figure 2.5: Schematic of a Solder Joint: (a) 2D; (b) 3D (Mookam and Kanlayasiri, 2018)

2.6 Sn-Pb Solder Alloy

For decades, Sn-Pb solders emerged as the prevailing standard within the electronics industry. The two most extensively deployed types of solder in PCB assembly are the near-eutectic Sn - 40Pb solder and the eutectic Sn - 37Pb solder. In the context of soldering, the versatility of substrate materials and components is facilitated by the Sn-37Pb melting point of 183 °C (Liu and Tu, 2020). Pb, being a critical constituent of eutectic solders, imparts numerous beneficial properties to Sn-Pb solders.

The incorporation of Pb to the Sn-Pb alloy contributes to a drop in the surface tension (Vianco, 1993). As mentioned earlier, the wetting abilities of solder are enhanced when it features a reduced surface tension. This enables it to effectively fill any apertures on the substrate where it is being soldered. The wetting angle of Sn on a Cu substrate was recorded as 35 °, while the wetting angle of the Sn-Pb alloy is 11 ° (Zeng and Tu, 2002). The reduced surface

tension and improved wetting angle of Sn, due to Pb's characteristics, are favorable for establishing a superior solder joint with improved adhesiveness.

Pb, an additive in Sn, inhibits the conversion of beta (β) Sn into alpha (α) Sn at conditions below 13 °C. In the event that this conversion takes place, it results in an upsurge of 27 % in volume, which undermines the framework of Sn under low-temperature conditions and induces fracture in solder joints (Peng, 2009). Moreover, at an exceptionally low temperature of 200 °C, the Sn-37Pb solder can reflow due to its low melting point of 183 °C (Zeng and Tu, 2002). Thus, the production of the Sn-Pb solder alloy is facilitated.

Ultimately, the solder's corrosion resistance is enhanced by Pb's corrosion resistance, which develops a dense and durable oxide coating that is chemically resistant and insoluble. It's also prohibited for Sn whiskers to develop since they can deteriorate solder joints (Wang, Ashworth and Wilcox, 2014). When these considerations are coupled with Pb's enhanced ductility, affordability, and ease of accessibility, it becomes a perfect alloying element when paired with Sn.

2.7 Sn-Bi Solder Alloy

Pb-free solder alloys, particularly Sn-Bi, Sn-Cu, Sn-In, and Sn-Zn, have drawn a lot of attention. Table 2.1 illustrates the eutectic temperatures of numerous binary Sn solders, whereas Table 2.2 summarizes the element costs for the solder alloys.

Table 2.1: Eutectic Temperatures of Binary Sn Solders (Abtew and Selvaduray, 2000)

Binary Eutectic Alloy	Eutectic Temperature (°C)
Sn - 58Bi	139
Sn - 0.7Cu	227
Sn - 52In	120
Sn - 37Pb	183
Sn - 9Zn	198.5

Table 2.2: Element Cost (Cheng, Huang and Pecht, 2017)

Element	Cost (USD/kg)
Sn	18.83
Bi	27.34
Cu	4.61
In	720
Pb	1.87
Zn	2.32

The low melting points of Sn-Bi Pb-free solder alloys are contributing to their growing recognition. Specifically, the eutectic temperature of the Sn-58Bi alloy is 139 °C, which is relatively lower contrasted to the 183 °C of the Sn-37Pb alloy. The primary advantage of Sn-Bi alloys over Sn-Pb alloys is that they require lower peak reflow temperatures during soldering, owing to their lower melting point. Lower peaks reflow temperatures are desirable as they minimise the likelihood of electronic component distortion, PCB board warping and delamination, as well as copper dissolution in molten solder. Thinner IMCs are the repercussions. Lower peaks reflow temperatures additionally assists reduce expenditures as they consume lesser heat during the SMT assembly operation (Dušek et al., 2022). According to research conducted by Pan et al. (2006) and Yang et al. (2016), Sn-58Bi solder alloys possess a shear strength of 44.70 MPa, which is roughly equivalent to that of traditional Sn-37Pb solder (45.50 MPa). This demonstrates that Sn-58Bi may be used as a substitute for traditional solder.

The brittleness of Sn-Bi alloys is their fundamental limitation, a consequence of the inherent features of Bi. The Bi's maximum solubility in Sn is approximately 21 wt.%, as indicated in Figure 2.6. After the concentration threshold is surpassed, Bi undergoes precipitation, resulting in the development of lamellae-like structures which hinder the solder ductility (Abtew and Selvaduray, 2000). Moreover, the liquidus temperature of Sn-Bi solder can be progressively reduced from 232 °C (the melting point of Sn) to 138 °C (at the eutectic composition of Sn-58Bi) through the incorporation of Bi into Sn, thereby reducing the soldering temperature (Wang et al., 2017a).

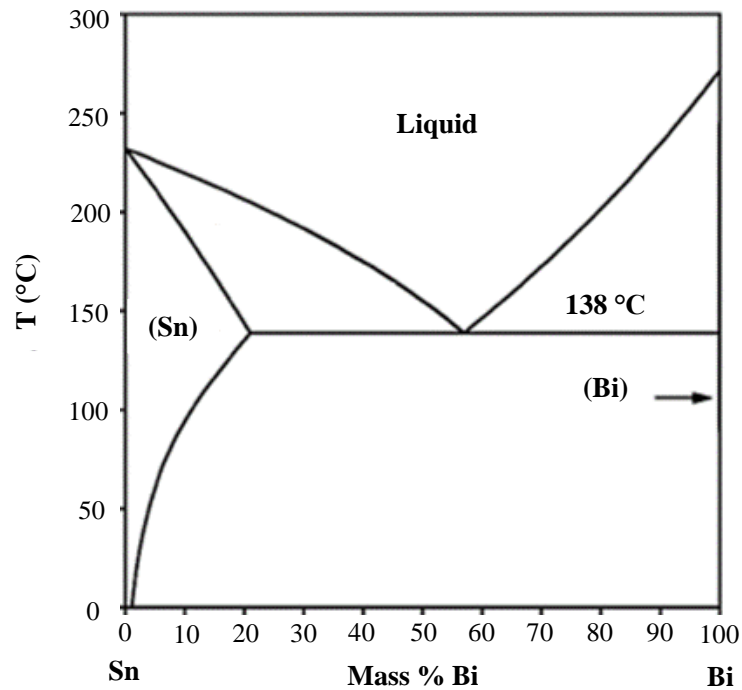


Figure 2.6: Sn-Bi Phase Diagram (Wang et al., 2017a)

2.8 Intermetallic Compounds (IMCs)

IMCs are characterised by their well-defined solid phases, which possess organised structures and consistent chemical constitutions; these phases are composed of two or more metals or semimetals (Jiang, He and Liu, 2018). The IMC that forms at the solder/substrate interface affects the joint's performance significantly. A metallurgical adhesion can be further improved by facilitating substantial wetting characteristics between the solder and the substrate, which can be accomplished by forming a thin and homogeneous layer of IMCs (Ting Tan, Wen Tan and Yusof, 2015).

On the contrary, an overabundance of thickness in these IMCs layer leads to heightened brittleness, thereby compromising the efficacy of the solder joint. Uncontrolled development of IMCs has detrimental impacts on the strength of solder joints, their resistance to thermal fatigue, and fracture toughness. Consequently, such development can potentially result in premature failures and brittle fractures (Aamir et al., 2017). Hence, it is imperative to manipulate the thicknesses of the IMC layers in order to optimize the reliability of solder joints.

An IMC layer will develop at the Sn-Bi/Cu interface when Sn-Bi alloys are soldered to a Cu substrate. Yang et al. (2016) claimed that this interface was where Cu_6Sn_5 and Cu_3Sn developed. Figure 2.7 illustrates the surface morphologies of Sn-58Bi/Cu. Bright gray regions in the Sn-58Bi solder represent Bi, while dark grey sections represent Sn, resulting in an interlocking lamellar structure (Mokhtari and Nishikawa, 2016).

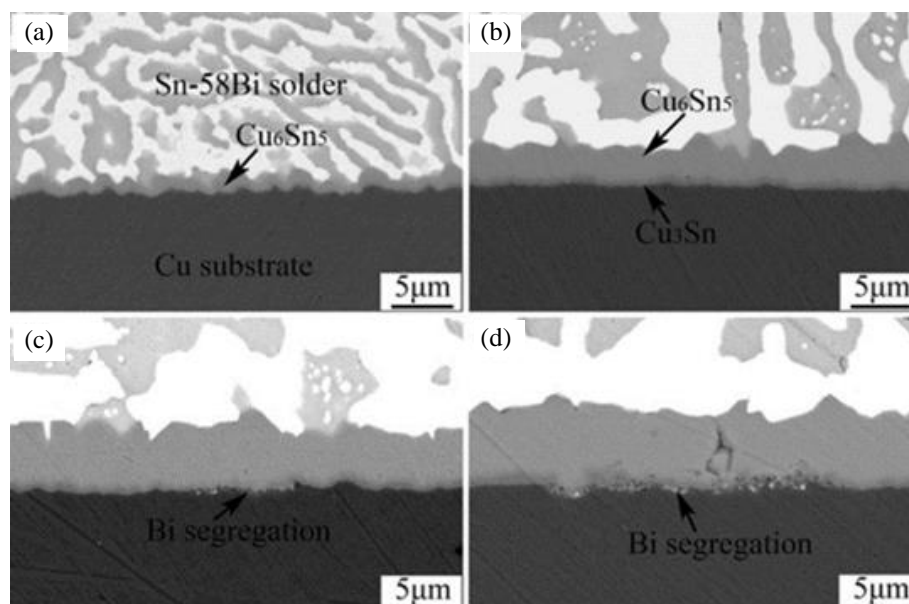


Figure 2.7: Surface Morphologies of Sn-58Bi/Cu (Zhang, Zou and Zhang, 2011)

As previously stated, during the reflow phase, the Sn-Bi alloy is heated above its melting point. Following flux depletion, the substrate is saturated with molten solder, which initiates Cu dissolution. The procedure commences with the development of a scallop-shaped $\eta\text{-Cu}_6\text{Sn}_5$ phase, which develops rapidly into a homogeneous thin layer subsequent to heterogeneous nucleation at the interface as demonstrated in Figure 2.7 (a). The continuous diffusion of Cu from the substrate through the thin Cu_6Sn_5 layer into the molten solder results in the development of a small Cu_6Sn_5 . Ostwald ripening occurs at the interface layer when smaller Cu_6Sn_5 IMCs redeposit onto larger adjacent Cu_6Sn_5 IMCs. Consequently, the thickness and coarseness of the Cu_6Sn_5 layer evolve progressively. An additional $\epsilon\text{-Cu}_3\text{Sn}$ phase, illustrated in Figure 2.7 (b), will form in the vicinity of the $\eta\text{-Cu}_6\text{Sn}_5/\text{Cu}$ layer as the heating process advances. This phenomenon arises due to the progressive enhancement of the

thermodynamic conditions for Cu_3Sn formation on the Cu substrate (Zhang, Zou and Zhang, 2011; Gain and Zhang, 2016a; Liu and Tu, 2020).

While Bi does not exhibit a direct contribution to the formation of IMCs, it does exert an influence on interface attributes. The dissolution of the Bi atoms into the Cu_6Sn_5 IMC layer results in their subsequent segregation at the $\text{Cu}_3\text{Sn}/\text{Cu}$ interface, as proposed by Zhang, et al. (2011). This occurs due to the fact that the larger Bi atoms within the IMC induce lattice deformation, which in turn stimulates the formation of cracks, as depicted in Figures 2.7(c) and 2.7(d) (Yoon, Lee and Jung, 2002; Yang et al., 2016).

2.9 Activated Carbon (AC)

AC is a common nanoparticle reinforcement used in the development of lead-free composite solders with improved properties. AC is distinguished by its substantial specific surface area and remarkable physical adsorption abilities due to its exceptionally porous structure, which derives from carbonaceous resources such as wood, bamboo, coconuts, coal, and petroleum (Yim and Kim, 2023). Said, et al. (2015) observed that the introduction of AC particles resulted in a reduction in the wetting angle between Sn-Cu-Ni and the Cu substrate from 40° to 22.16° with 1.00 wt.% of AC. This, in turn, enhanced the adhesion and integrity of the solder joint.

According to research conducted by Said, et al. (2015), Ramli, et al. (2016) and Izwan et al. (2015), incorporating AC particles into Sn-Cu-Ni solder can significantly reduce the thickness of IMCs layer by retarding their growth. It is proposed that transitioning Cu atoms from the substrate to the molten Sn-Cu-Ni solder is impeded by obstacles imposed by the even dispersion of AC particles along a diffusion channel of IMC layer. The existence of AC modifies the morphology of the IMC layer in addition to decreasing its thickness. As the concentration of AC increases, the scalloped IMC layer, which resembles a needle shape, transforms into a continuous structure, as demonstrated in Figure 2.8. As the needle-like scalloped structure tends to promote brittle fractures, the variations in the morphology of the IMC layer are regarded as advantageous.

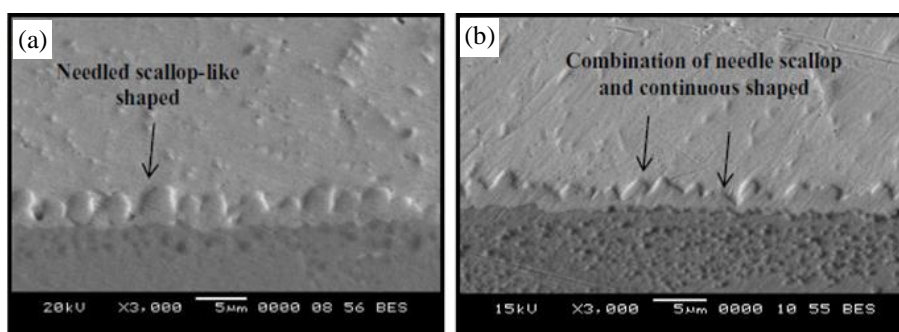


Figure 2.8: SEM Micrograph of cross-sectional view of interfacial IMC: (a) Sn-Cu-Ni; (b) Sn-Cu-Ni-1.0AC (Ramli et al., 2016)

Furthermore, an increase in AC particle incorporation results in a substantial optimization of the shear strength of Sn-Cu-Ni solder, as determined by Ramli et al (2016). Sayyidah (2015) bolstered this discovery with further evidence by showcasing improvements in the shear strength of Sn-Cu upon the incorporation of AC particle reinforcement. It has been documented that the main driver contributing to enhanced shear strength is the reduction in IMC thickness. The solder joint's strength is compromised by an increase in IMC thickness, as the susceptibility of a thicker IMC layer to failure is exacerbated by the presence of a greater number of microcracks and dislocations (An and Qin, 2014).

Given the recent developments regarding the complete ban on Pb in PV modules and the novel use of BC as an additive to Sn-Bi solder, there is currently no available literature on Sn-Bi solder reinforced with materials like BC. Previous research on similar reinforcements, such as AC, focused on other solder alloys and did not account for the low melting point and cost-effectiveness of Sn-Bi solder. Additionally, these studies were conducted prior to the latest Pb ban, with Sn-Bi now being considered the only viable Pb-free alternative by PV manufacturers.

2.10 Bamboo Charcoal (BC)

BC, derived from mature bamboo species, is a viable substitute for AC due to its availability and sustainability. Bamboo provides a substantial reservoir of biomass due to its exceptionally rapid growth rate (Chaturvedi et al., 2024). AC and BC are mainly differentiated by their production processes. AC is subjected

to steam or other gases in addition to the high-temperature treatment that it undergoes to produce BC (Thao, 2023). BC is widely recognized for its exceptional conductivity and porous structure, which enable it to possess a substantial adsorption capacity and a massive specific surface area. Carbonization treatment temperature-induced changes in the BC's structure, including the transition from an insulator to a semiconductor or conductor, coupled with an enlargement of the pores (Subyakto, Budiman and Pari, 2017).

BC is an extremely promising candidate for use in the semiconductor industry due to its exceptional features. Recent research has investigated the possibility of using these materials as electrodes in dye-sensitized solar cells (DSSC). The operational process of DSSCs initiates with the elevation of electron energy from its lowest state to a higher state via the absorption of radiation by a photosensitizer in the form of a dye. The excited electrons are subsequently introduced into the TiO₂ electrode's conduction band and advance in the direction of the anode's current receiver. Electricity provision to an electrical device is facilitated by the connection (Sharma, Sharma and Sharma, 2018).

Researchers Isa, et al. (2016) discovered that by incorporating BC into TiO₂, photocatalytic performance and the functionality of the solar cell were enhanced through increased dye absorption and excited electron emission in response to sunlight. The narrow band gap and disordered surface layer caused by BC's outstanding conductivity and large effective surface area are responsible for this. However, there has been no research conducted to examine the impact of BC on solder joint performance.

2.11 Shear Strength

A wide range of research initiatives have been devoted to the improvement of shear strength in Sn-Bi solder joints with the aim of creating innovative solder compounds. A substantial influence on the shear strength of these joints is exerted by both the microstructure and the development of the IMCs layer (Singh et al., 2018). The viability of enhancing solder joint strength through the integration of minute quantities of alloying elements into Sn-Bi solder alloys has been validated. Several potential alloying candidates are detailed in Table 2.3. In contrast, the solder joint's properties commence to degrade at

concentrations surpassing the maximum allowable threshold for additional elements.

Table 2.3: Alloying Elements in Sn-Bi alloy

Alloying Elements	Maximum Weight Percentage (wt.%)	References
Vanadium (V)	0.6	(Yang et al., 2019)
Silver (Ag)	0.5	(Kang, Rajendran and Jung, 2021)
Indium (In)	0.5	(Mokhtari and Nishikawa, 2013)
Magnesium (Mg)	0.4	(Chen et al., 2023)
Zinc Oxide (ZnO)	0.4	(Rajendran, Kang and Jung, 2021)
Yttrium Oxide (Y ₂ O ₃)	1.0	(Liu, et al., 2010)
Aluminum Oxide (Al ₂ O ₃)	1.0	(Hu et al., 2015)

The contribution of each alloying element on optimizing the shear strength of Sn-Bi solder is comparable. Sn-Bi solder first undergoes microstructure refinement through the addition of an alloying elements. While Bi and Sn are abundant in a coarse, alternating eutectic morphology, the introduction of additional alloying elements refines it into a lamellar structure. The nucleation sites provided by the alloying elements are responsible for the solder matrix refinement. The existence of nucleation sites facilitates nucleation circumstances that occur during solidification by minimizing the free energy barrier (Rajendran, Kang and Jung, 2021). The presence of multiple grain boundaries within the refined microstructure of Sn-Bi hinders the movement of grains, thereby increasing the force required to initiate dislocation motion. This, in turn, contributes to the solder's improved shear strength. However, Sn-Bi solder alloys microstructure eventually becomes coarser due to the presence of surplus alloying elements, which reduces the fluidity of the molten solder and their functionality as nucleation sites during the reflowing phase (Yang et al., 2019).

Apart from that, shear strength can be strengthened by incorporating alloying elements into the solder alloy via dispersion strengthening to reduce the thickness of the IMCs layer. Cu_6Sn_5 IMCs with alloying elements tend to have smaller grains to hinder dislocation motion. Furthermore, the alloying elements inhibit the atom diffusion process by pinning the IMCs and hindering the IMCs layer from developing. Preserving a thin Cu_6Sn_5 IMCs layer under monitoring and ensuring a uniform distribution of Cu_6Sn_5 IMCs can effectively prevent grain dislocation along the solder joint boundaries, thereby improving shear strength (Hu et al., 2015; Rajendran, Kang and Jung, 2021).

The shear strength of solder joints decreases over time due to the thickening of the IMC and the coarsening of phases within the solder matrix under isothermal aging conditions. As time progresses, the Cu_6Sn_5 IMC layer transitions from a scallop-type structure to a planar one, while Cu_3Sn form at the $\text{Cu}_6\text{Sn}_5/\text{Cu}$ interface, leading to an overall increase in the interfacial IMC thickness (Liu et al., 2012; Wang et al., 2017a; 2017b). Additionally, extended exposure to elevated temperatures accelerates the diffusivity of atoms, vacancies, and interstitials, promoting the growth and coarsening of grains with fewer boundaries to hinder dislocation motion (Ma and Suhling, 2009).

2.12 Fractography

According to Table 2.4, there are three main ways in which solder joints can experience shear failure. Mode 1 illustrates the ductile fracture mechanism through the penetration of the solder matrix. As the crack travels through the solder matrix and subsequently the IMC layer in Mode 2, it exemplifies a combined ductile-brittle fracture mechanism. Brittle Mode 3 fractures are those that propagate entirely within the interfacial IMC layer (Mohd Salleh et al., 2012; Rajendran, Hwang and Jung, 2020).

Table 2.4: Fracture Failure Modes

Fracture Mode	Fracture Mechanism
Mode 1 – In Solder Region	Ductile Fracture
Mode 2 – Between Solder/IMC Interface	Mixed Ductile-Brittle Fracture
Mode 3 – In IMC Interface	Brittle Fracture

Mode 3, depicted in Figure 2.9 (a and b), is a brittle failure of the Sn-Bi solder joint, characterised by a flat and smooth fracture surface. This mode, in which the fracture propagates through the IMCs layer, is primarily caused by the brittle segregation of Bi at the interface (Yang et al., 2016).

The ductility of the Sn-Bi solder joint can be enhanced by incorporating adequate alloying elements to it. As previously mentioned, the inclusion of alloying elements refines the microstructure. Shear stress induces distortion and dispersion of Sn-Bi solder into these smaller grains that are directionally diverse. The dispersion of solder greatly impedes the advancement of fractures and enhances the ductility of the matrix (Zhang et al., 2019). The development of IMC layer is further impeded through the incorporation of alloying elements. Fracture consequently takes place primarily within the Sn-Bi solder matrix, exhibiting enhanced ductility but lower strength than the IMC layer (Mode 1). Several examples of ductile failure caused by the alloying additives in Sn-Bi solder are illustrated in Table 2.5. A bulge fracture morphology with dimples, signifying ductile deformation of the Sn-rich phase, is indicative of ductile failure (Rajendran, Kang and Jung, 2021). For instance, bulge fractures with dimples in Sn-Bi solder doped with 0.5 wt.% Al_2O_3 are depicted in Figure 2.9 (c and d).

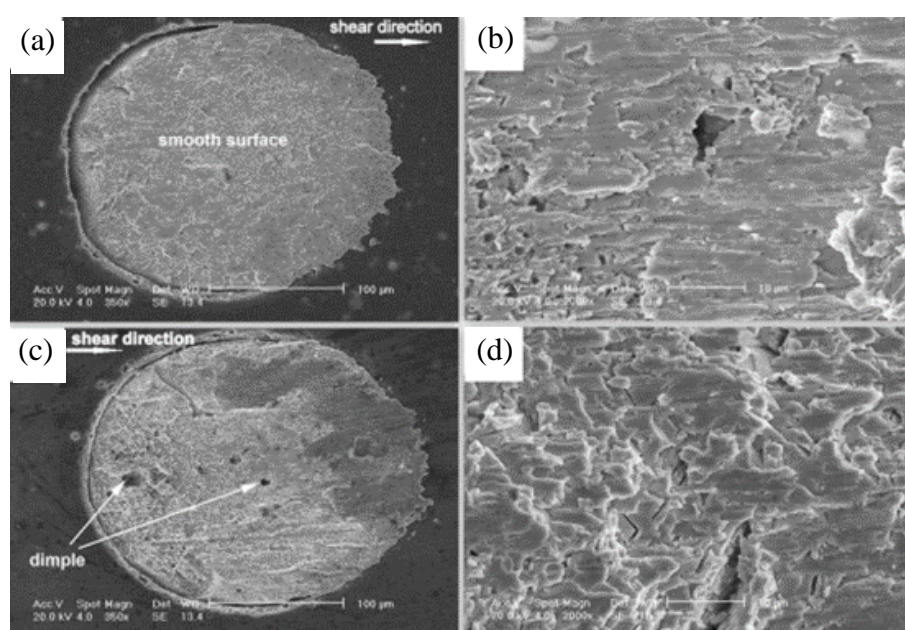


Figure 2.9: Fracture Surfaces at Different Magnification: (a and b) Sn-Bi Solder; (c and d) Sn-Bi solder with 0.50 wt.% Al_2O_3 (Hu et al., 2015)

Table 2.5: Alloying Elements that Induce Ductile Failure Mode in Solder Matrix

Alloying Elements	Maximum Weight Percentage (wt.%)	References
Vanadium (V)	0.4	(Yang, et al., 2019)
Magnesium (Mg)	0.2	(Chen et al., 2023)
Zinc Oxide (ZnO)	0.05	(Rajendran, Kang and Jung, 2021)
Aluminum Oxide (Al ₂ O ₃)	0.5	(Hu et al., 2015)

Elevated alloying element concentrations reduce ductility, which in turn increase cleavage fracture. Generally, these cleavage fractures represent the brittle Bi phase (Rajendran, Kang and Jung, 2021). Furthermore, the development of the IMC layer is further suppressed. As a result, the propagation of fractures is prolonged, and energy absorption is increased. The solder joint's ultimate shear stress is thereby greatly increased (Sayyadi and Naffakh-Moosavy, 2019). Consequently, the Sn-Bi solder and the IMC layer exhibit a ductile-brittle mixed fracture mode. Nevertheless, an overabundance of alloying elements may gradually transform the fracture characteristics of the solder from combined ductile - brittle to brittle, thereby reducing its shear strength.

The primary factor contributing to the change in failure mode is the coarsening of the IMC as a result of age, which results in the displacement of the fracture location toward the substrate. Figure 2.10 illustrates that the Kirkendall effect induces the formation of voids within the Cu₃Sn IMC layer that develops during isothermal aging, which is characterised by brittleness. The layer is rendered porous as a result of this phenomenon, which substantially reduces the strength of the solder adhesive bond with the substrate. As the duration of aging increases, the rate of growth of the Kirkendall voids is substantially increased. Consequently, the porous layer of Cu₃Sn IMC is unable to achieve the necessary mechanical and electrical adhesion, which increases the probability of brittle fracture and eventual delamination of the solder joint (Choi and Oh, 2001; Peng, Monlevade and Marques, 2007; Wang et al., 2017b).

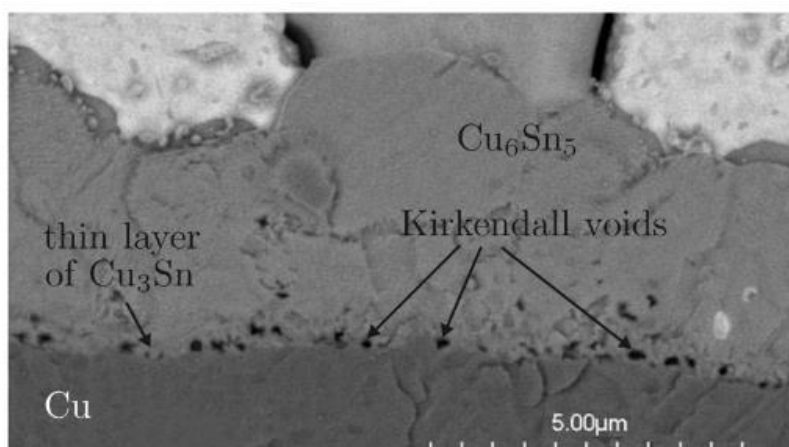


Figure 2.10: Kirkendall Voids within Cu_3Sn IMC layer (Weinberg and Böhme, 2009)

2.13 Summary

Sn-Pb solder alloys give rise to significant environmental and health concerns. Sn-58Bi lead-free solder alloys are considering becoming a viable substitute due to their low melting point properties. During reflow soldering, IMCs develop in the Sn-58Bi/Cu interfacial layers, in addition to brittle Bi segregation. This resulted in reduced strength and brittle fractures in the solder joint. Nevertheless, it has been documented that the adequate incorporation of alloying elements improves the strength and ductility of solder joints through microstructural refinement and suppression of IMCs layer development.

Given the recent developments concerning the complete ban on toxic Pb in PV modules and the innovative use of BC as an additive to Sn-Bi solder, there is currently no literature available on Sn-Bi solder reinforced with materials like BC. The only documented application of BC found in the literature is in the semiconductor industry, where it has been employed as an electrode material for DSSC to improve their photocatalytic performance. Previous research on similar reinforcements, such as AC, has focused exclusively on other solder alloys, like Sn-Cu-Ni, to improve solder joint performance.

CHAPTER 3

METHODOLOGY AND WORK PLAN

3.1 Introduction

The research methodology comprised four consecutive parts: (i) Sample Preparation; (ii) Specimen Preparation; (iii) Reflow Soldering and Accelerated Aging; (iv) Shear Testing and (v) Microstructural Fracture Analysis.

3.2 Sample Preparation

Commercial Sn-58Bi solder paste from ChipQuik with an average particle diameter of 25 - 45 μm was used while the reinforcement was activated BC supplied by Future Food. Sn-58Bi-xBC composite solder samples were created by incorporating varying wt.% of activated BC nanoparticles powder into the Sn-58Bi solder paste, where x represented 0.00, 0.25, 0.50, 0.75, and 1.00 wt.%, respectively. The pure Sn-58Bi alloy without activated BC reinforcement served as a control variable for comparison purposes. Thus, a total of five sets of samples with varying activated BC contents were prepared as demonstrated in Figure 3.1. The mass of activated BC powder required for each set was determined based on Equation 3.1. Subsequently, each set of composite solder samples was stirred for 10 minutes to ensure homogeneity and prevent agglomeration.



Figure 3.1: Sn-58Bi-xBC Composite Solder Samples Preparation

$$\begin{aligned} & \text{Mass of BC required (g)} && \text{(Equation 3.1)} \\ & = \frac{\text{wt.\% of BC}}{\text{wt.\% of BC} + \text{wt.\% of Sn-58Bi}} \times \text{Mass of Sn - 58Bi (g)} \end{aligned}$$

3.3 Specimen Preparation

For this study, a single lap shear joint specimen was necessary according to ASTM D1002 (2019): Apparent Shear Strength of Single Lap Joints Adhesively Bonded Metal Specimens by Tension Loading. A blank PCB, referred to as a Cu substrate was cleaned with ethanol and distilled water after being sectioned into dimensions of 50 mm x 10 mm x 1.5 mm (length, width, and thickness) using shear machine (Yee, Wong and Issabayeva, 2019). Following this, a stencil with an aperture area of 10 x 10 mm² and a thickness of 0.2 mm was positioned on a PCB piece, enabling precise and consistent screen printing of the composite solder sample at the designated location. After removing the stencil, another PCB piece was stacked on top to form a single lap shear joint specimen, as depicted in Figure 3.2.

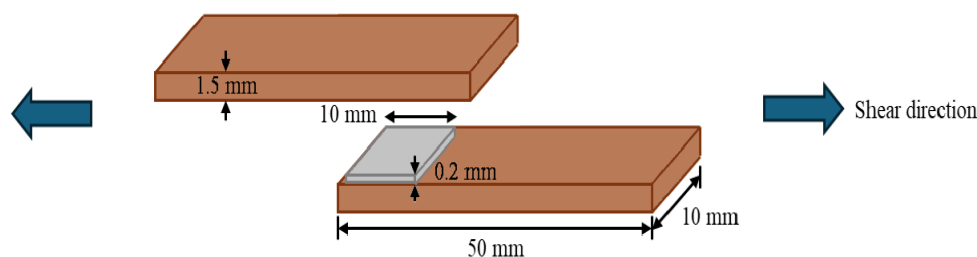


Figure 3.2: Single Lap Shear Joint Specimen

3.4 Reflow Soldering and Accelerated Aging

The reflow profile provided by ChipQuik for Sn-58Bi solder assembly was depicted in Figure 3.3. Reflow soldering was carried out in a programmable furnace. Test specimens were positioned in the furnace and subjected to preheating, starting from 25 °C (room temperature) and gradually increasing to 138 °C, held for approximately 210 seconds. Subsequently, the temperature was raised to the peak reflow temperature of around 165 °C and maintained for 30 seconds during the reflow phase. Eventually, the specimens were permitted to cool to 138 °C before being taken out of the oven to further cool down to room

temperature. Due to time constraints, the specimens for accelerated aging were heat-treated at 120 °C in an oven for 7 and 14 days.

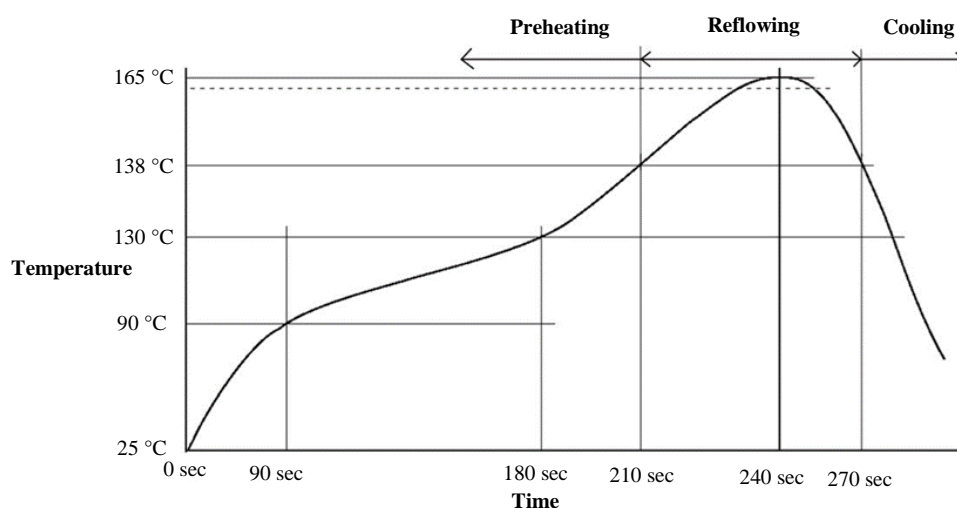


Figure 3.3: Reflow Profile for Sn-58Bi Solder Assembly (ChipQuik, 2024)

3.5 Shear Testing

The Universal Tensile Machine (Shimadzu Autograph AGS-X Series) as shown in Figure 3.4 was used to evaluate the shear strength of solder joints in accordance with ASTM D1002. Before initiating the test, the crosshead speed was set to 1.2 mm/min. The specimen was then placed between upper and lower tensile fixtures, and the test began with pulling the adhered specimens in tension until failure. This tension applied shear stress across the entire adhered area, as illustrated in Figure 3.2 by the orientations of two arrows representing shear stress. Throughout the test, the applied force on the specimen was monitored, revealing a stress-strain diagram. 3 specimens were tested for each condition to obtain an average result.



Figure 3.4: Universal Testing Machine (Shimadzu Autograph AGS-X Series)

3.6 Microstructural Fracture Analysis

The fractured surfaces of Cu/Sn-58Bi-xBC/Cu solder joints ($x = 0.00$ to 1.00 wt.%) were sectioned into $10 \times 10 \text{ mm}^2$ samples following shear testing. After that, the samples were positioned on metal stubs after coating with gold (Au) and investigated with a Hitachi S-3400 N scanning electron microscope (SEM) as shown in Figure 3.5. The identification of the fracture mechanism was accomplished by employing secondary electron (SE) imaging with an accelerating voltage of 15 kV . The fracture surface's elemental composition was then determined using energy-dispersive X-ray (EDX) analysis.

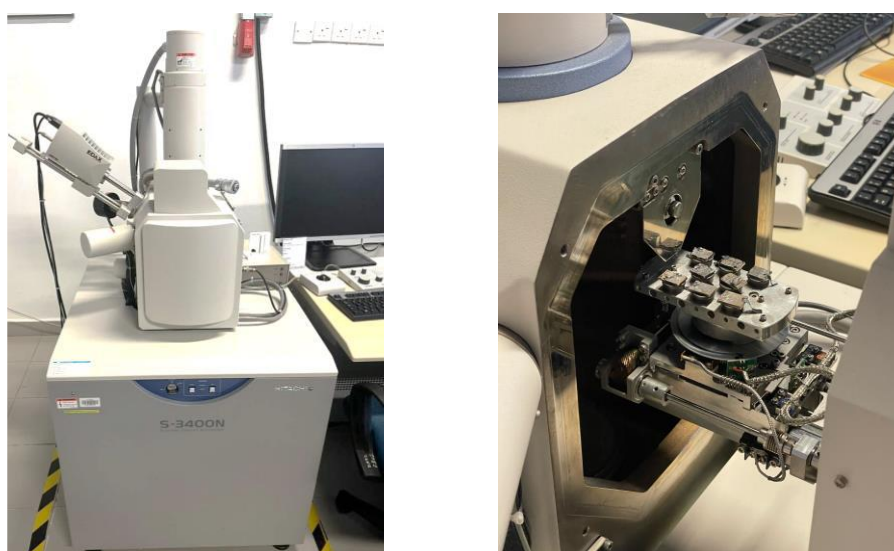


Figure 3.5: Hitachi S-3200 N Scanning Electron Microscope (SEM)

3.7 Summary

The summarised experimental procedures were depicted in the flowchart presented in Figure 3.6.

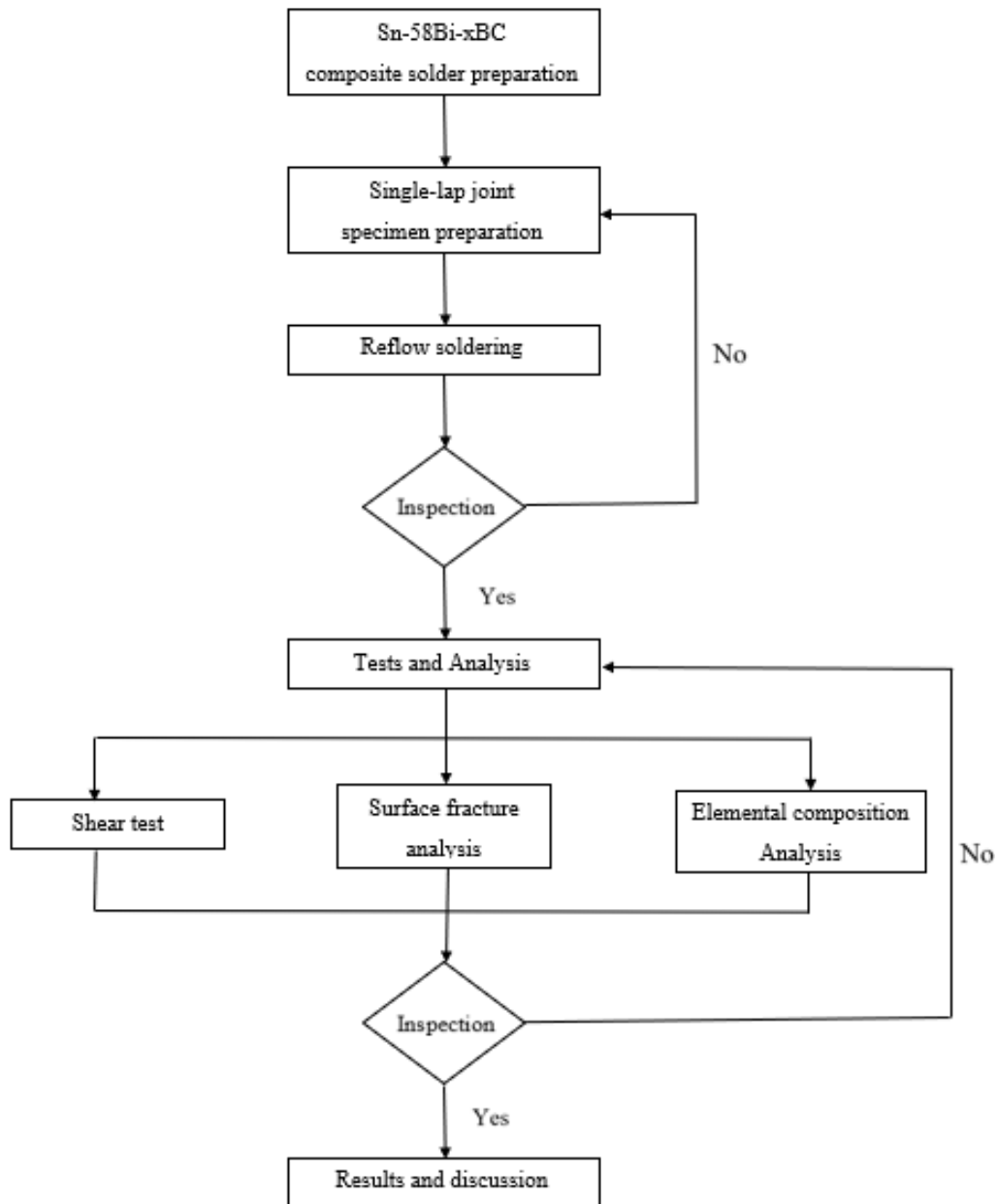


Figure 3.6: Flowchart of Methodology

CHAPTER 4

RESULTS AND DISCUSSION

4.1 Shear test

Figure 4.1 showed the shear strengths for Sn-58Bi alloy reinforced by varying amounts of activated BC. Pan et al. (2006) reported that the published shear strength of the conventional Sn-37Pb solder alloy was 45.50 MPa, which was nearly equivalent to the 45.68 MPa shear strength of Sn-58Bi obtained in the as-reflowed condition. When 1.00 wt.% of activated BC was introduced as a reinforcement, the shear strength of the Sn-58Bi alloy increased by about 21.67 %, reaching 55.58 MPa. The findings demonstrated that the Sn-58Bi alloy achieved its highest shear strength with the addition of 1.00 wt.% activated BC. However, due to time constraints, the optimal amount of activated BC for use remained inconclusive.

As mentioned in Section 2.9, a similar trend was observed with the addition of AC, which enhanced the shear strength of Sn-Cu-Ni. Furthermore, this insight aligned with Section 2.11, which indicated that the shear strength of Sn-58Bi increased with adequate reinforcement, such as Mg, ZnO and Al₂O₃. This indicated that activated BC was a more favourable reinforcement option, offering both sustainable benefits and the ability to enhance the solder's shear strength to an impressive 55.58 MPa, surpassing the conventional standardized strength of Sn-37Pb used in PV module applications. Samples that had been accelerated aging at 120 °C for 7 and 14 days, respectively, followed the general trend of increased shear strength with increasing amounts of activated BC additions. According to the Hall-Petch relationship, which depicts grain refinement as a strengthening mechanism, asserts that materials with smaller grain sizes demonstrate a higher mechanical strength due to the increased number of grain boundaries that impede dislocation movement (Yang et al., 2013; Chantaramanee and Sungkhaphaitoon, 2021; Kang, Rajendran and Jung, 2021).

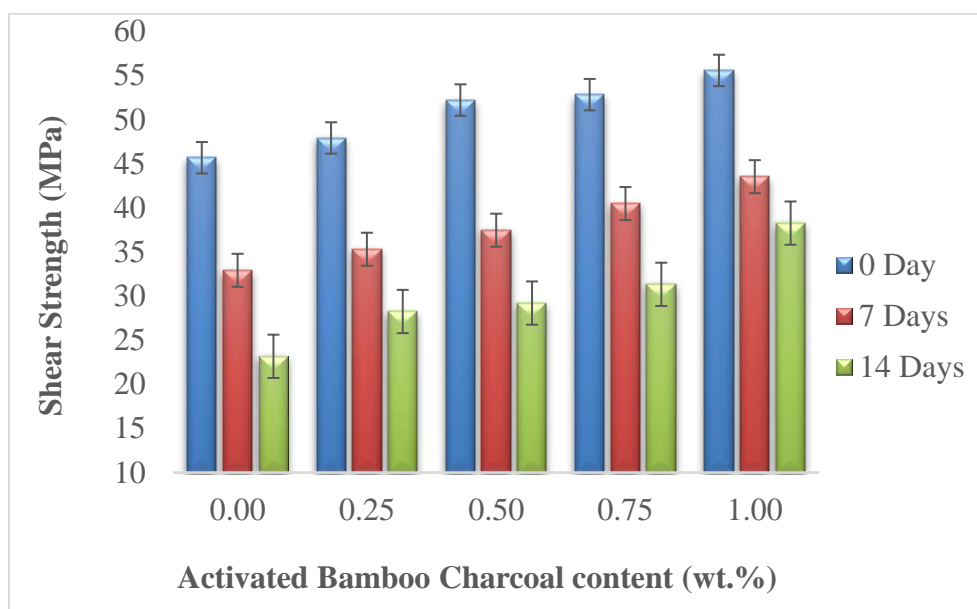


Figure 4.1: Shear Test Results for Sn-58Bi Alloy with Varying Amounts of Activated BC Content

The coarse microstructure of Sn-58Bi solder, which was primarily characterised by the brittle Bi phase, can be effectively refined by the incorporation of activated BC. The adsorption capabilities of activated BC were enhanced by its large specific surface area and porous nature, which enabled it to establish extensive contact with the coarse Bi phase in the solder matrix (Song et al., 2021). This adsorption suppressed the coarsening of the solder microstructure, which would otherwise induced brittleness. The weight percentages of activated BC added were proportional to the degree of solder microstructural refinement. As the activated BC content increased, a more homogeneous distribution of phases within the solder was achieved, with a greater number of phase boundaries that effectively impeded crack propagation, while smaller Bi precipitates reduced stress concentration areas. As a consequence, the force necessary to initiate dislocation motion increased, leading to an increase in shear strength.

With accelerated aging at 120 °C, the shear strength of both pure and reinforced Sn-58Bi solders decreased as the duration of aging increased. However, the declined in shear strength was more pronounced in solder joints without activated BC. After 14 days of accelerated aging, the Sn-58Bi solder exhibited a substantial 49.28 % decreased in shear strength, whereas the solder

containing 1.00 wt.% activated BC exhibited only a 31.14 % decrease. Kurtz et al (2009) reported that thermal exposure of rack-mounted PV modules was comparable to aging at a constant temperature in the hottest cities. Thus, these variances indicated that the reliability of Sn-58Bi solder in prolonged exposure of high-temperature environments could be enhanced by incorporating activated BC nanoparticles.

In the Sn-Bi system, Bi had negligible solubility for all elements, as indicated by the phase diagram. As a result, the introduction of activated BC primarily enhanced the solder joints through dispersion strengthening and heterogeneous nucleation (Wang et al., 2017a). The enhanced shear strength of aged Sn-58Bi solder joints that were reinforced with activated BC nanoparticles through dispersion strengthening can be attributed to the ability of activated BC to regulate grain ripening, interfacial IMC growth, and Kirkendall void formation (Zhou et al., 2017; Rajendran, Hwang and Jung, 2020). Activated BC possibly prevented segregation of Bi precipitates by providing heterogeneous nucleation sites. This would have mitigated the impact of grain ripening during accelerated aging, which weakens solder joints because larger particles/clusters were more vulnerable to stress concentrations. Similar findings had been observed with the addition of SiC and ZrO₂ nanoparticle reinforcements in Sn-58Bi solder. Due to the increased heterogeneous nucleation sites provided by the reinforcements that obstructed phase boundary movement, the average eutectic size decreased following accelerated aging, indicating a refined solder microstructure (Gain and Zhang, 2016c; Kang, Rajendran and Jung, 2021).

Furthermore, activated BC may have been adsorbed at the IMC layer, reducing the diffusion rates between Cu and Sn, thereby preventing excessive interfacial growth. This, in turn, reduced the formation of Kirkendall voids, which can be led to thermal fatigue failure due to brittleness (Ho, Yang and Kao, 2007; Guo et al., 2020). The SEM images of the interface between the Cu substrate and Sn-58Bi solder were presented in Table 4.1, both in the as-reflowed condition and after 14 days of accelerated aging. Little variation was observed in the thickness of the IMCs at the interface of all samples in the as-reflowed condition. However, the IMC layers exhibited substantial growth following 14 days of accelerated aging.

The IMC interfacial layer and Kirkendall voids were depicted in Figure 4.2, while the IMC thickness measurements after reflowing and aging were illustrated in Figure 4.3, which was obtained using ImageJ software. In the as-reflowed condition, the Sn-58Bi alloy had an IMC thickness of 0.9075 μm , which decreased by about 26.89 % when 1.00 wt.% activated BC was added as reinforcement. After 14 days of accelerated aging, the Sn-58Bi solder exhibited a substantial 82.36 % increase in IMC thickness. Samples that had been subjected to accelerated aging at 120 °C for 7 and 14 days, respectively, followed the general trend of decreased IMC thickness with increasing amounts of activated BC additions, and increased IMC thickness with prolonged accelerated aging, consistent with the provided explanation.

Excessive interfacial layer growth during accelerated aging can weakened the solder-substrate bond due to the inherently brittle nature of the IMC, causing degraded joint strength. Besides, the bonding was further weakened by the formation of Kirkendall voids. This insight was consistent with the findings of Kang, Rajendran and Jung (2021), who demonstrated that incorporating Ti and ZnO nanoparticle reinforcements into Sn-58Bi effectively impeded the diffusion of Sn atoms towards the interface by acting as pinning sites, resulting in a reduction in the thickness of the IMC layer. Preserving a thin IMCs layer under monitoring and ensuring a uniform distribution of IMCs can effectively prevent grain dislocation along the solder joint boundaries, thereby improving shear strength.

Table 4.1: Intermetallic Morphology After Reflow and After 14 Days of Aging

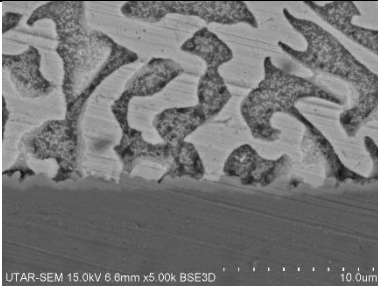
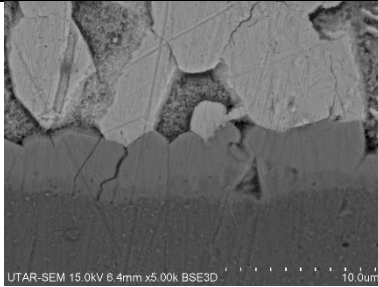
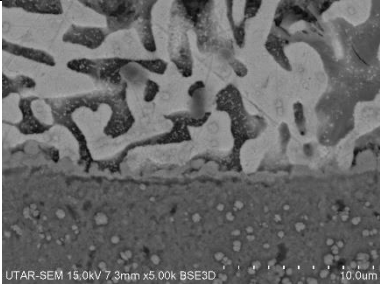
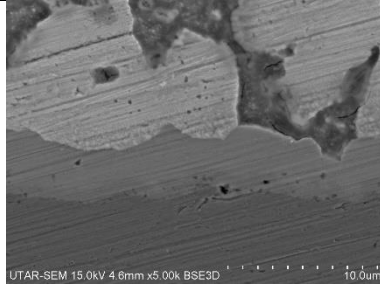
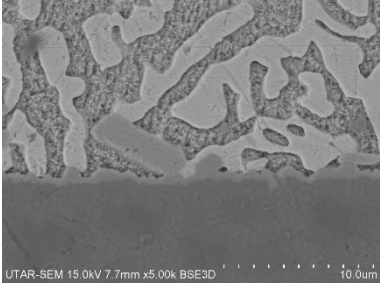
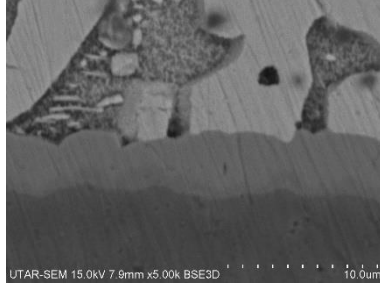
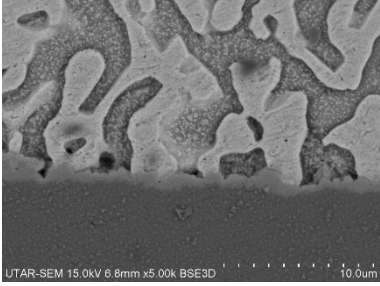
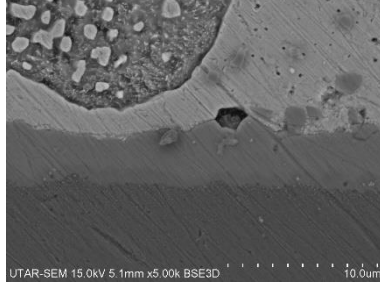
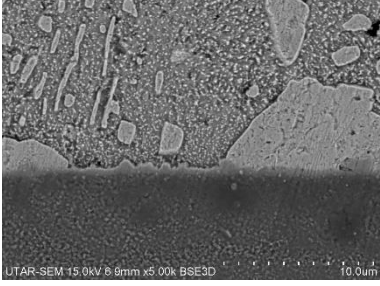
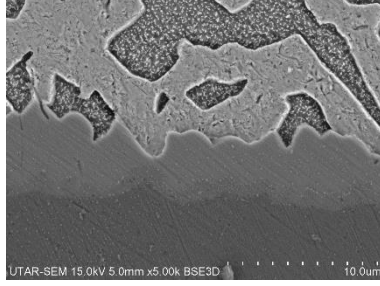
	0 Day (As-Reflowed)	14 Days of Accelerated Aging
Sn-Bi		

Table 4.1 (Continued)

Sn-Bi + 0.25 wt.% BC	 <p>UTAR-SEM 15.0kV 7.3mm x5.00k BSE3D 10.0um</p>	 <p>UTAR-SEM 15.0kV 4.6mm x5.00k BSE3D 10.0um</p>
Sn-Bi + 0.50 wt.% BC	 <p>UTAR-SEM 15.0kV 7.7mm x5.00k BSE3D 10.0um</p>	 <p>UTAR-SEM 15.0kV 7.9mm x5.00k BSE3D 10.0um</p>
Sn-Bi + 0.75 wt.% BC	 <p>UTAR-SEM 15.0kV 6.8mm x5.00k BSE3D 10.0um</p>	 <p>UTAR-SEM 15.0kV 5.1mm x5.00k BSE3D 10.0um</p>
Sn-Bi + 1.00 wt.% BC	 <p>UTAR-SEM 15.0kV 6.6mm x5.00k BSE3D 10.0um</p>	 <p>UTAR-SEM 15.0kV 5.0mm x5.00k BSE3D 10.0um</p>

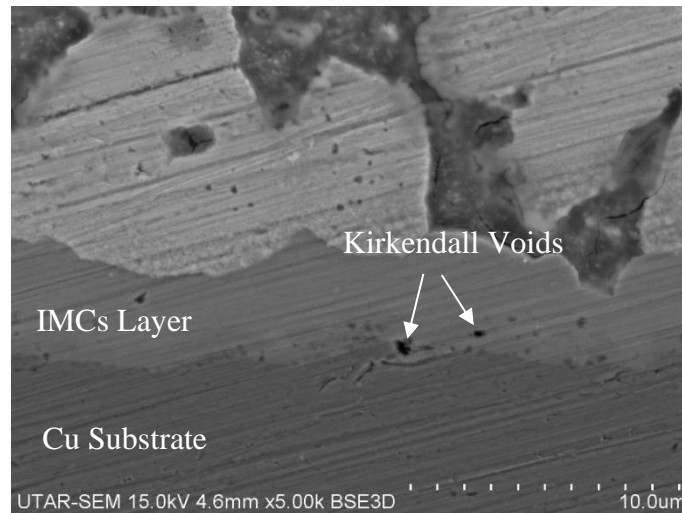


Figure 4.2: IMCs and Kirkendall Voids in 14-Day Accelerated Aging Samples with 0.25 wt.% Activated BC

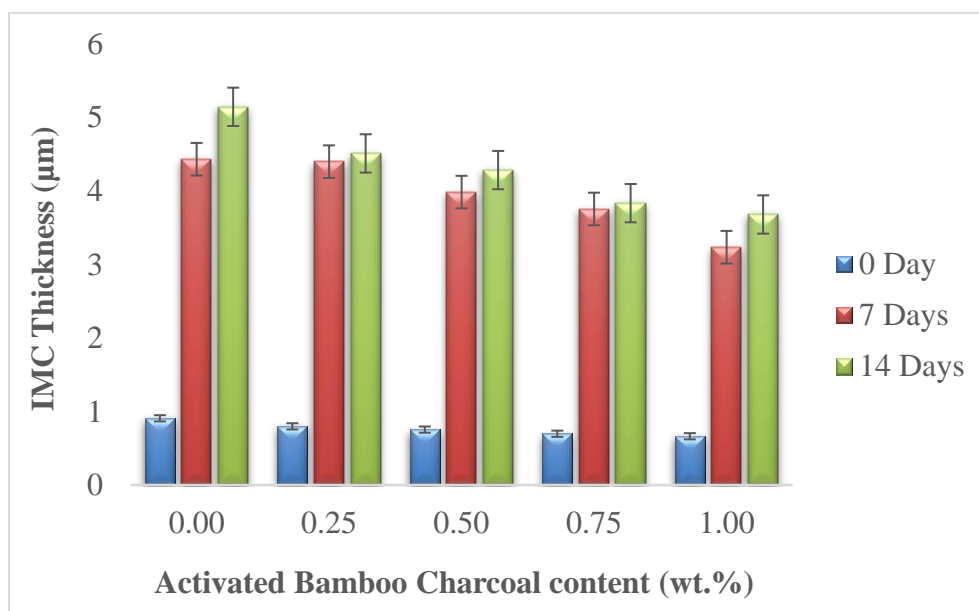


Figure 4.3: IMCs Thickness with Varying Amounts of Activated BC Content

4.2 Fracture Mode

Solder joints can undergo shear failure through three primary modes as illustrated in Figure 4.4. Mode 1 referred to the ductile fracture mechanism through the penetration across the solder matrix. Bulge fractures with noticeable dimples characterised the resulting cracked surface. As the crack travelled through the solder matrix and subsequently the IMC layer in Mode 2, it exemplified a combined ductile-brittle fracture mechanism. Less cleavage

facets and voids characterised the fracture surfaces of this mode. Brittle Mode 3 fractures were those that propagated entirely within the interfacial IMC layer. In this mode, surfaces with fractures appeared smooth or with more cleavage facets (Rajendran, Hwang and Jung, 2020).

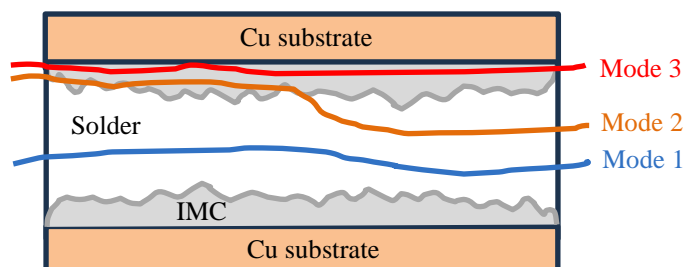


Figure 4.4: Failure Modes of Solder Joint

Among these modes, Mode 1, the in-solder failure mode, was preferred, as illustrated in Table 4.2. This type of failure occurred within the solder matrix, which was advantageous because it provided protection for electronic components in packaging and can be readily repaired through solder joint reflowed processes. In contrast, Mode 3, the IMC failure mode, was undesirable because components soldered onto the IMC layer were vulnerable to the damaging effects of fracturing within that layer.

Table 4.2: Fracture Failure Modes

Failure Mode	Conditions
Mode 1 – In Solder Region	Desirable
Mode 2 – Between Solder/IMC Interface	Neutral
Mode 3 – In IMC Interface	Undesirable

The shear strength results presented in Figure 4.1 were further supported by Table 4.3, showing the types of failure modes observed, and Table 4.4, which detailed the percentage of failure modes. The IMC failure mode exhibited the lowest shear strength as a result of its intrinsic brittleness, followed by the combined solder/IMC failure mode and the in-solder failure mode, which exhibited the highest shear strength due to its ductility. The absorption and redistribution of stress among the refined grains that were directionally diverse

was facilitated by ductility, which enabled substantial plastic deformation of the solder prior to fracture, particularly when subjected to shear stresses. This redistribution increased overall shear strength by reducing the likelihood of localized failures, which were common in brittle IMC (Zhang, Sun and Liu, 2019; Rajendran, Hwang and Jung, 2020; Chen et al., 2023).

From Table 4.4, the likelihood of in-solder failure mode increased with higher activated BC content and decreased with longer accelerated aging durations. Table 4.5 presented the images depicting the predominant failure modes observed in Sn-58Bi solder alloys reinforced with varying amounts of activated BC content. Specifically, the probability of in-solder failure increased as the activated BC content increased, particularly in the as-reflowed condition and after 7 days of accelerated aging. However, only 33% of the samples containing 1.00 wt.% activated BC exhibited solder failure mode after 14 days of accelerated aging.

In the as-reflowed samples with 1.00 wt.% activated BC, 100 % failed via Mode 1 (in the ductile solder region). Continued accelerated aging for 7 and 14 days resulted in a decline in ductility and, consequently, shear strength, with failures via Mode 1 decreasing to 67 % and 33 %, respectively. For samples containing 0.75 wt.% activated BC, 33 % of the as-reflowed samples and 67 % of those subjected to 7 days of accelerated aging failed via Mode 2 (at the ductile solder and brittle IMC interface). After 14 days of accelerated aging, 100 % of the samples failed via Mode 2, indicating an increase in brittleness and a reduction in shear strength.

Further, 67 % of Sn-58Bi solder samples failed via Mode 3 (at the brittle IMC interface) for both as-reflowed and 7-day accelerated aging conditions. Continued accelerated aging for 14 days resulted in 100 % failure via Mode 3, indicating an undesirable brittle fracture. No failures via Mode 3 were observed in as-reflowed samples containing 0.50 wt.% or more of activated BC, and the 7- and 14-day accelerated-aged samples did not exhibit Mode 3 failures when the activated BC content was at 0.75 wt.% or higher, demonstrating that greater activated BC addition increased ductility, but prolonged accelerated aging significantly reduced the ductility of solder joints. The reduction in ductility

could be caused by the grain ripening and excessive IMCs development as presented in Figure 4.3, which ultimately resulted in lower reliability.

All these findings were consistent with the trend observed in the shear test results. With the addition of BC, there was a higher likelihood of Mode 1 fractures occurring in the solder region, indicating an increased in ductility and, consequently, greater shear strength of the solder joint.

Table 4.3: Types of Failure Modes Observed


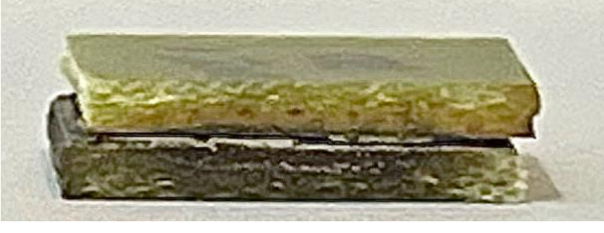

1. In-solder Failure Mode	
2. Mixed Mode (solder/IMC failure)	
3. IMC Failure Mode	

Table 4.4: Percentage of Failure Modes for Sn-58Bi Reinforced by Different Weight Percentages of Activated BC

0 Day (As-Reflowed)					
Failure Mode	Sn-Bi	Sn-Bi + 0.25 wt.% BC	Sn-Bi + 0.50 wt.% BC	Sn-Bi + 0.75 wt.% BC	Sn-Bi + 1.00 wt.% BC
Solder Mode	0%	0%	33%	67%	100%
IMC/Solder Mode	33%	67%	67%	33%	0%
IMC Mode	67%	33%	0%	0%	0%

Table 4.4 (Continued)

7 Days of Accelerated Aging					
Failure Mode	Sn-Bi	Sn-Bi + 0.25 wt.% BC	Sn-Bi + 0.50 wt.% BC	Sn-Bi + 0.75 wt.% BC	Sn-Bi + 1.00 wt.% BC
Solder Mode	0%	0%	0%	33%	67%
IMC/Solder Mode	33%	33%	67%	67%	33%
IMC Mode	67%	67%	33%	0%	0%

14 Days of Accelerated Aging					
Failure Mode	Sn-Bi	Sn-Bi + 0.25 wt.% BC	Sn-Bi + 0.50 wt.% BC	Sn-Bi + 0.75 wt.% BC	Sn-Bi + 1.00 wt.% BC
Solder Mode	0%	0%	0%	0%	33%
IMC/Solder Mode	0%	33%	67%	100%	67%
IMC Mode	100%	67%	33%	0%	0%

Table 4.5: Predominant Failure Modes of Sn-58Bi Reinforced by Different Weight Percentages of Activated BC
















Aging Duration Composition	0 Day (As- Reflowed)	7 Days of Accelerated Aging	14 Days of Accelerated Aging
Sn-Bi			
Sn-Bi + 0.25 wt.% BC			
Sn-Bi + 0.50 wt.% BC			

Table 4.5 (Continued)

Sn-Bi + 0.75 wt.% BC			
Sn-Bi + 1.00 wt.% BC			

4.3 Fractography

Figure 4.5 and 4.6 depicted the micrograph and elements presented in activated BC nanoparticles. It had an average particle size of approximately 18 μm and was composed of 100% carbon, C. Figure 4.7 showed the carbon content in Sn-58Bi samples reinforced with varying amount of activated BC in the as-reflowed condition. It revealed a positive trend, indicating that the atomic percentage of carbon increased with the weight percentage of activated BC reinforcement.

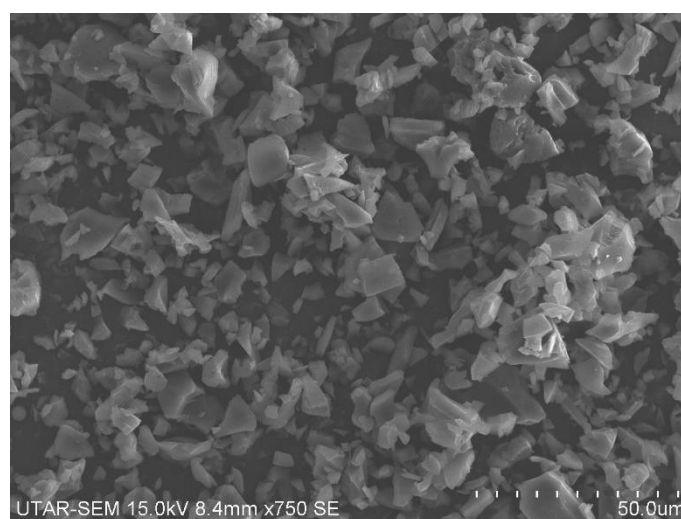


Figure 4.5: Micrograph of Activated BC Nanoparticles

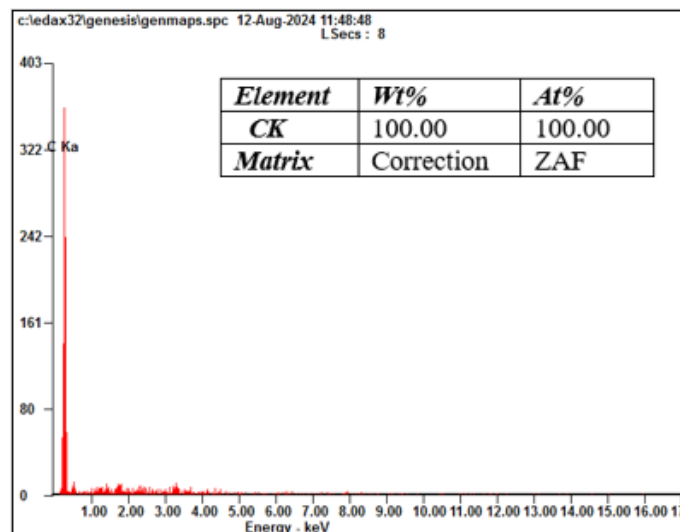


Figure 4.6: Element of Activated BC

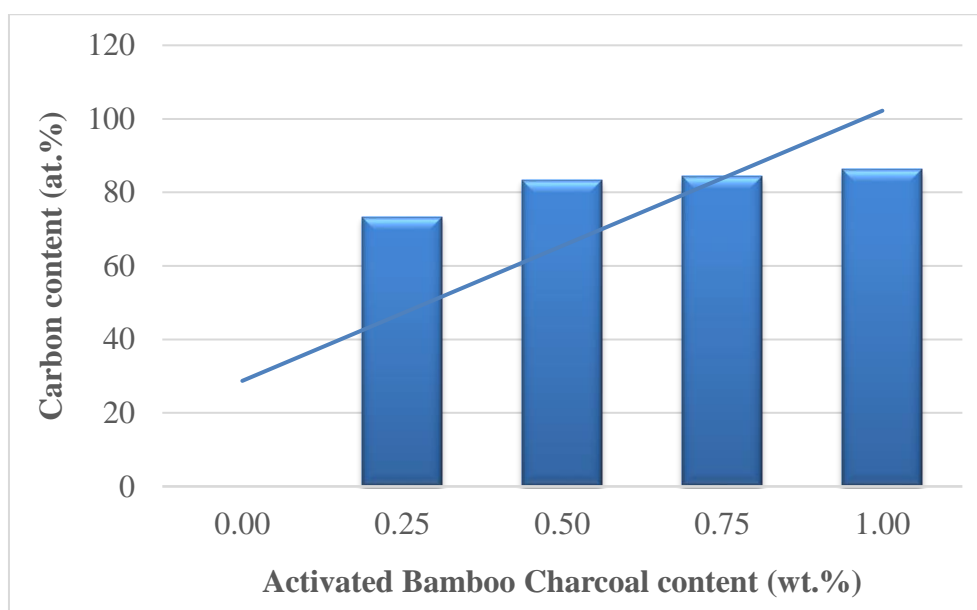


Figure 4.7: Carbon content in different activated bamboo charcoal reinforced Sn-58Bi (as-reflowed condition)

The failure modes showed in Table 4.3 and 4.4 were further supported by data from Figures 4.8 to 4.17, which illustrated the changes in fracture behaviour when different amounts of activated BC were added to Sn-58Bi under various accelerated aging conditions. Across all conditions, similar trends were observed: the ductility of the solder increased with the addition of activated BC but decreased with prolonged aging durations. Table 4.6 presented the morphological features and observations with increasing activated BC addition.

For the as-reflowed Sn-58Bi-xBC samples (Figures 4.8 to 4.10), the Sn-58Bi sample exhibited a predominantly flat and smooth fracture surface, indicating brittle fracture. Higher magnification SEM image (Figure 4.11) revealed intergranular fractures, consistent with the characteristics of brittle fracture. This brittle failure mode was primarily due to the segregation of large Bi atoms at the interface, causing lattice deformation and leading to concentrated stress during shear tests (Chen, McCloskey and O'Mathuna, 2006; Yang et al., 2016). However, with the addition of 0.50 wt.% activated BC, dimples appeared on the fracture surface, signifying increased ductility. Further increasing the activated BC content to 1.00 wt.% resulted in more pronounced, elongated dimples with greater depth and size, indicating substantial plastic deformation (Chen et al., 2018; Han et al., 2019; Lu et al., 2023). These dimples were formed by microvoids that developed and coalesced during plastic deformation, tearing the solder surface in the shear direction and creating tear ridges (Rajendran, Hwang and Jung, 2020). These findings were consistent with Section 2.12, which discussed the fracture behaviour of pure Sn-Bi solder, where a flat and smooth fracture surface transformed into a ductile failure with a dimpled structure upon the addition of 0.50 wt.% Al_2O_3 .

Prolonged accelerated aging led to an increase in cleavage facets due to the formation of a continuous Bi-rich layer, suggesting a reduction in ductility (Wang et al., 2019a; 2019b). The samples aged for 14 days showed more cleavage facets than those aged for 7 days, indicating an increased in brittleness, which aligned with this explanation. Besides that, the dimples in the 7- and 14-day aged samples appeared as voids without elongation or a parabolic shape because they were accompanied by the presence of cleavage facets. Void was the area of stress concentration. This observation indicated a mixed fracture mode, which exhibited both ductile and brittle properties (Yang et al., 2022; Gao et al., 2023).

Both the 7- and 14-day aged samples also followed the general trend of increasing activated BC content, similar to the as-reflowed samples. In the 7-day aged Sn-58Bi-xBC samples (Figures 4.12 to 4.14), the addition of activated BC resulted in a decreased in both void size and cleavage facets. Similarly, in the 14-day aged Sn-58Bi-xBC samples (Figures 4.15 to 4.17), there was a

decreased in void size and a significant reduction in cleavage facets with the addition of more activated BC. Smaller voids resulted in less concentrated stress, allowing the material to withstand greater deformation. In both cases, these changes indicated an increased in ductility and the fracture behaviour transitioned from brittle to a mixed brittle-ductile mode with the presence of voids.

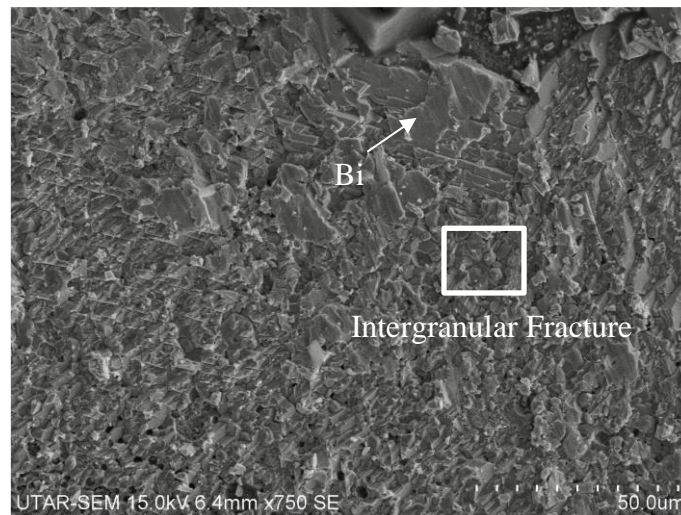


Figure 4.8: Fracture Surface of As-Reflowed Samples with 0.00 wt.% Activated BC

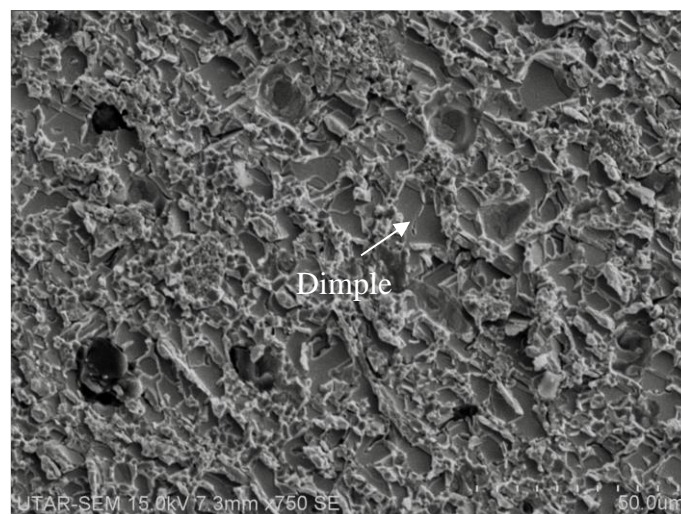


Figure 4.9: Fracture Surface of As-Reflowed Samples with 0.50 wt.% Activated BC

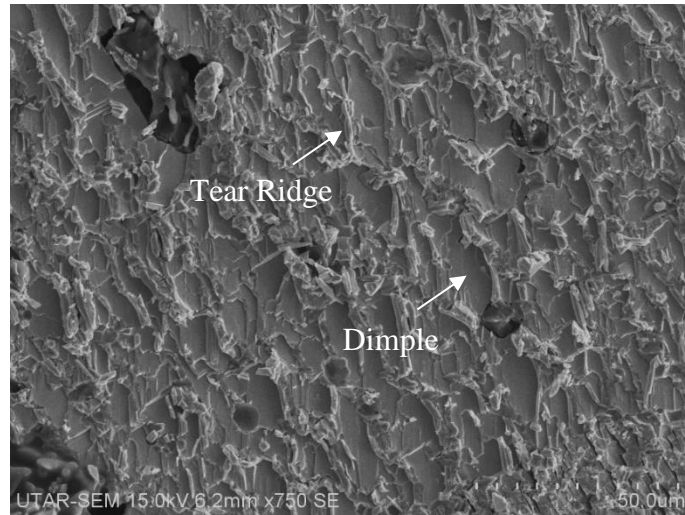


Figure 4.10: Fracture Surface of As-Reflowed Samples with 1.00 wt.% Activated BC

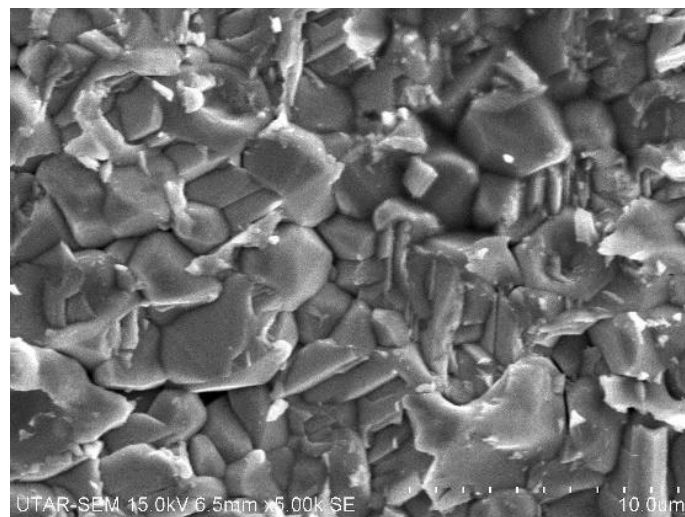


Figure 4.11: Intergranular Fracture of As-Reflowed Samples with 0.00 wt.% Activated BC

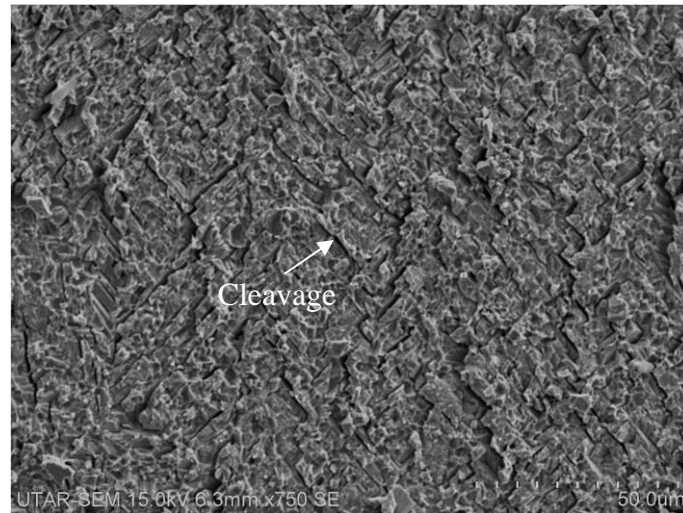


Figure 4.12: Fracture Surface of 7-Day Accelerated Aging Samples with 0.00 wt.% Activated BC

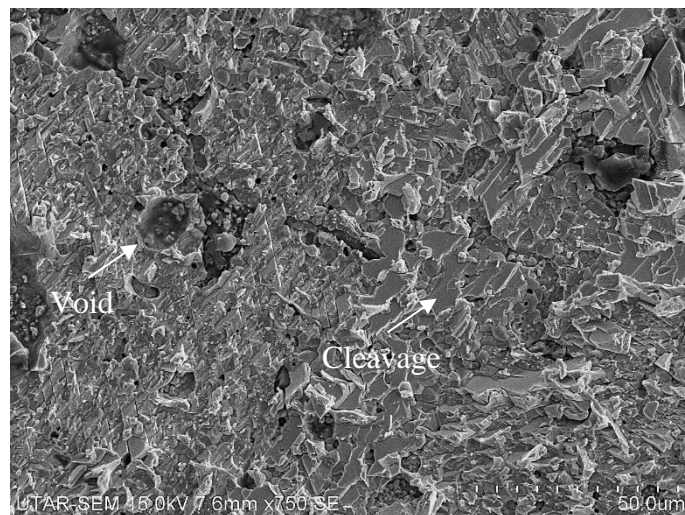


Figure 4.13: Fracture Surface of 7-Day Accelerated Aging Samples with 0.50 wt.% Activated BC

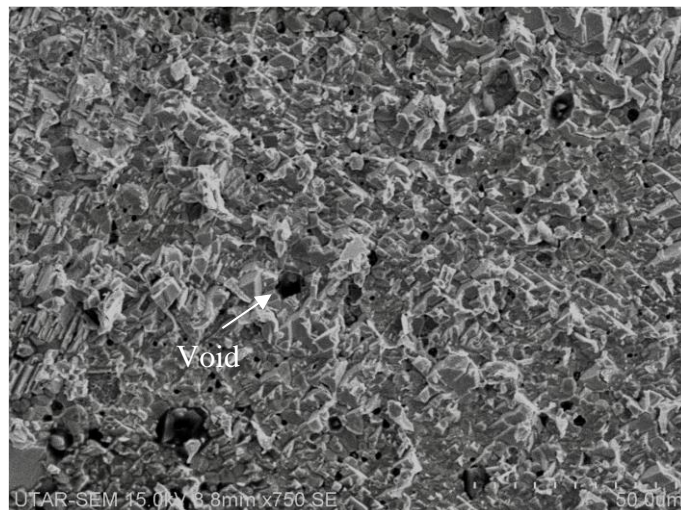


Figure 4.14: Fracture Surface of 7-Day Accelerated Aging Samples with 1.00 wt.% Activated BC

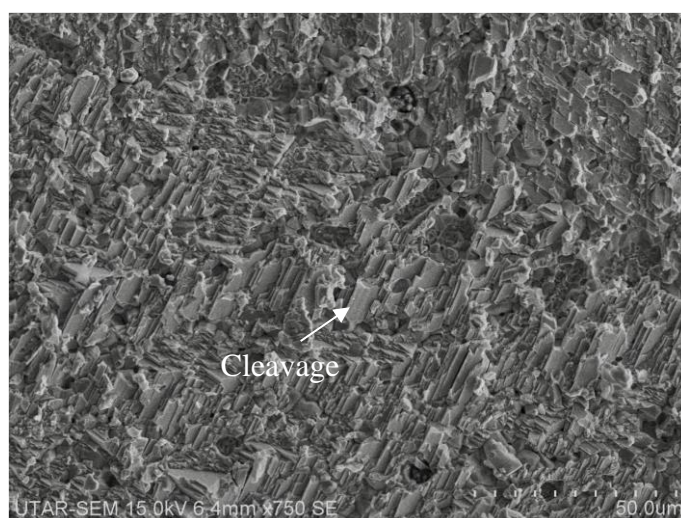


Figure 4.15: Fracture Surface of 14-Day Accelerated Aging Samples with 0.00 wt.% Activated BC

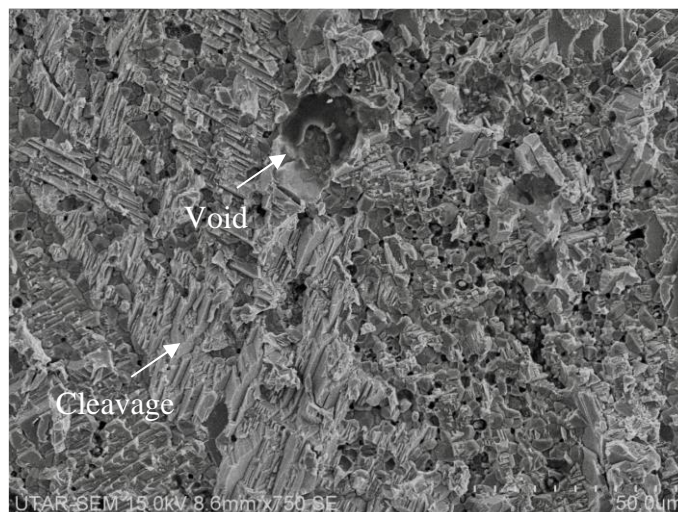


Figure 4.16: Fracture Surface of 14-Day Accelerated Aging Samples with 0.50 wt.% Activated BC

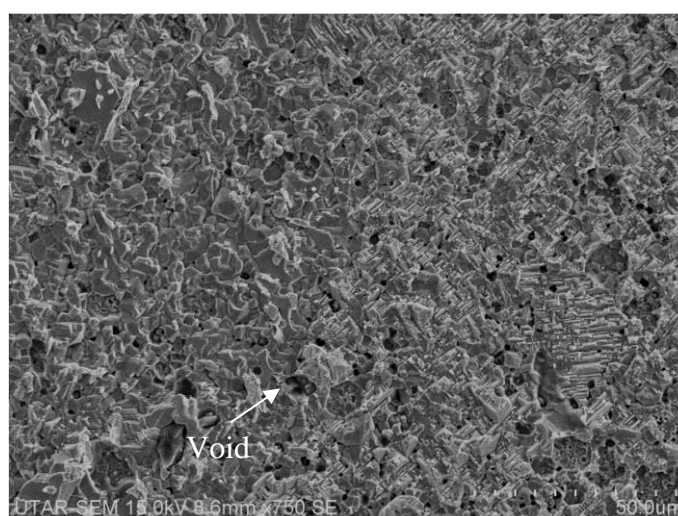


Figure 4.17: Fracture Surface of 14-Day Accelerated Aging Samples with 1.00 wt.% Activated BC

Table 4.6: Morphological Features and Observations with Increasing Activated BC Addition

Features	Observation (s)
Dimples	Elongated dimples with greater depth and size
Inclusions	Carbon content increases
Cleavage	Amount of cleavage facets decrease
Voids	Smaller voids

Inclusion particles, identified as carbon from the BC element in Figures 4.18 to 4.21, were observed in the dimple areas of most activated BC-containing samples. During the solidification of the solder, the activated BC acted as supplementary nucleation sites, promoting a more refined solder microstructure. This refinement helped to distribute localized stress more uniformly during fracture when external stress was applied, leading to the formation of dimples with significant plasticity (Yang et al., 2020). Fine Bi precipitates were also observed in the reinforced samples, indicating that activated BC particles adsorbed and effectively suppressed the segregation of the typically coarse Bi phase, enhancing both ductility and shear strength. Figures 4.22 to 4.24 showed a slight increase in particle size as the aging process progresses, due to Ostwald ripening.

All pure Sn-58Bi samples demonstrated brittle fracture behaviour with deep cleavage facets, while reinforced samples exhibited shallow facets with increasing aging duration. In general, samples containing more activated BC had fewer facets, and dimple colonies grew larger with the addition of activated BC.

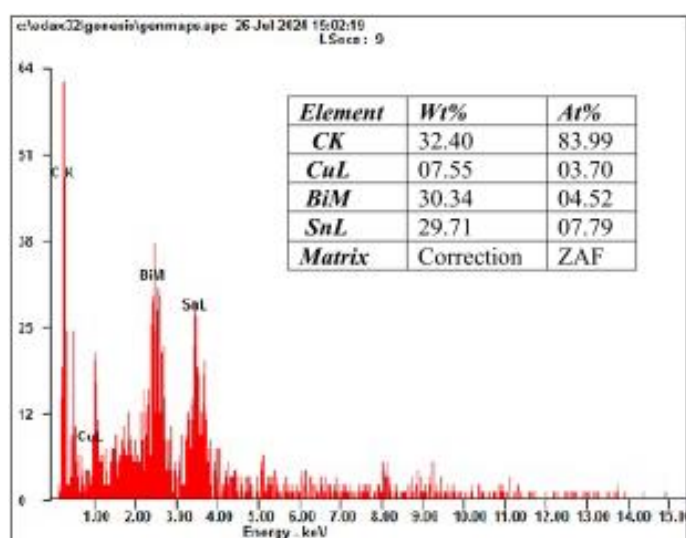


Figure 4.18: Carbon Content Elements in Dimples of As-Reflowed Samples with 0.25 wt.% Activated BC

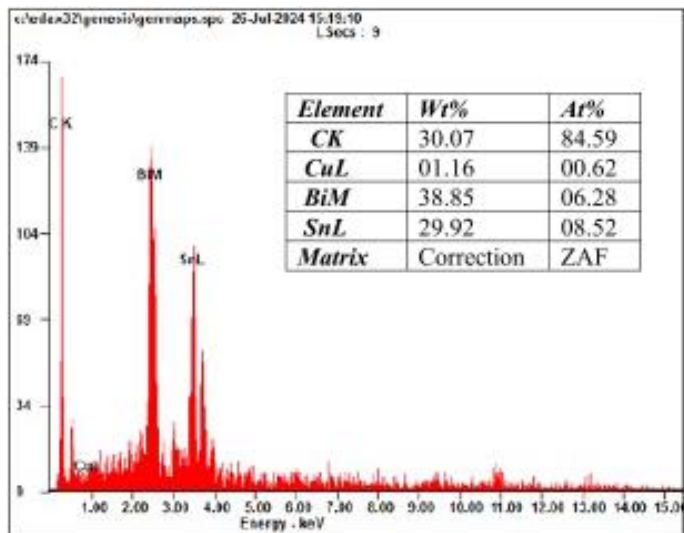


Figure 4.19: Carbon Content Elements in Dimples of As-Reflowed Samples with 0.50 wt.% Activated BC

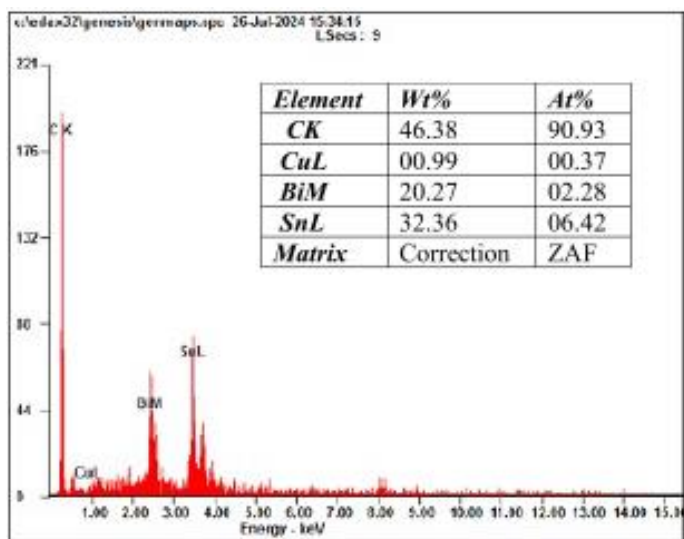


Figure 4.20: Carbon Content Elements in Dimples of As-Reflowed Samples with 0.75 wt.% Activated BC

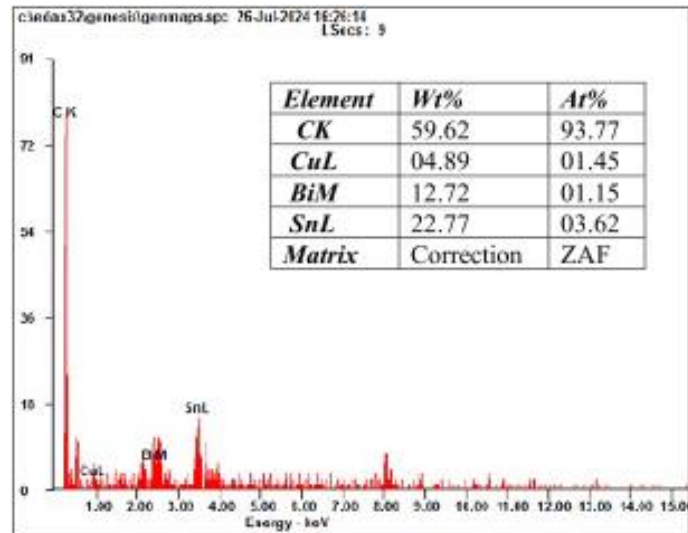


Figure 4.21: Carbon Content in Dimples of As-Reflowed Samples with 1.00 wt.% Activated BC

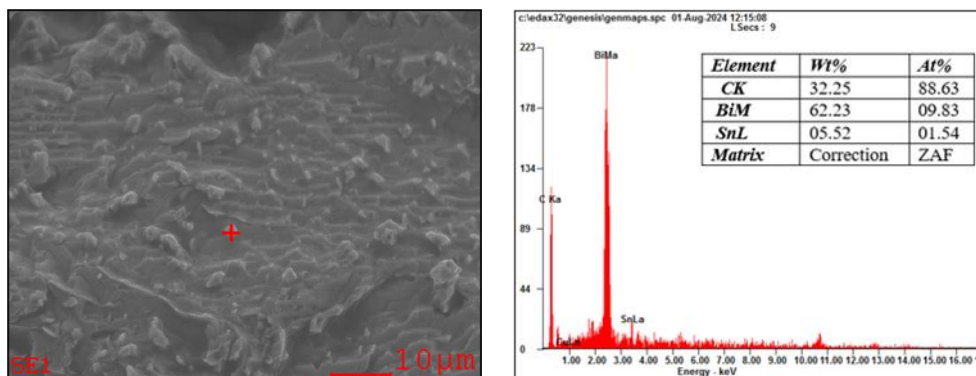


Figure 4.22: Fine Bi Precipitate (Sn-58Bi + 1.00 wt.% Activated BC) in As-Reflowed Condition

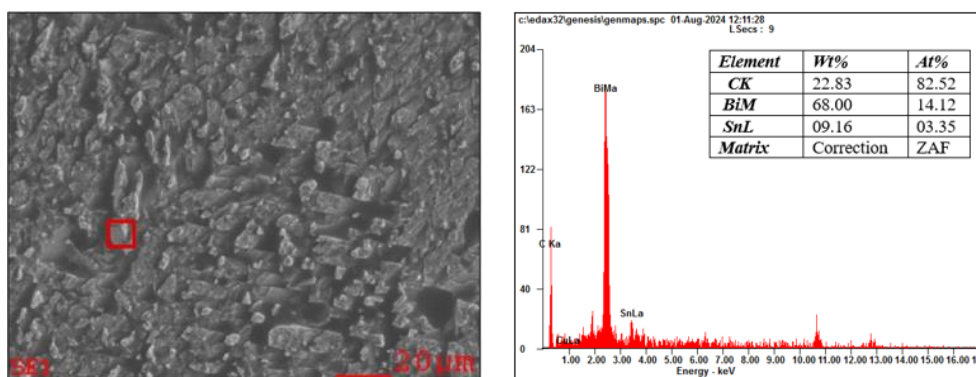


Figure 4.23: Fine Bi Precipitate (Sn-58Bi + 1.00 wt.% Activated BC) in 7-Day Accelerated Aging Condition

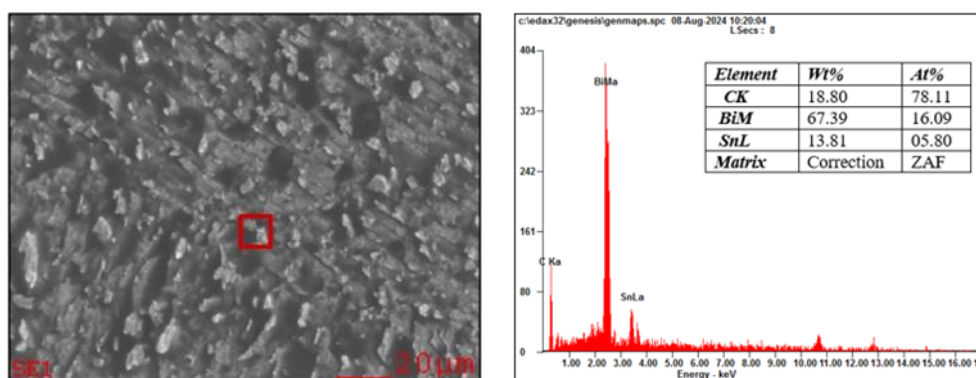


Figure 4.24: Fine Bi Precipitate (Sn-58Bi + 1.00 wt.% Activated BC) in 14-Day Accelerated Aging Condition

4.4 Summary

The shear strength of the Sn-58Bi alloy improved with the addition of activated BC, as predicted by the Hall-Petch relationship, but decreased with longer aging durations. In the as-reflowed condition, the shear strength of Sn-58Bi was 45.68 MPa, increasing by 4.90 %, 14.32 %, 15.67 %, and 21.67 % with the addition of 0.25 wt.%, 0.50 wt.%, 0.75 wt.%, and 1.00 wt.% of activated BC, respectively. After 7 days of accelerated aging, the shear strength decreased to 32.92 MPa, but it still increased by 7.26 %, 13.82 %, 22.99 %, and 32.26 % with the same additions of activated BC. After 14 days of accelerated aging, the shear strength further decreased to 23.17 MPa, but it increased by 21.92 %, 26.07 %, 35.22 %, and 65.17 % with the respective additions of 0.25 wt.%, 0.50 wt.%, 0.75 wt.%, and 1.00 wt.% of activated BC.

However, the reduction in shear strength was more pronounced in solder joints without activated BC. After 7 days of accelerated aging, the Sn-58Bi solder exhibited a substantial decrease of 32.92 % in shear strength, while the solder containing 1.00 wt.% activated BC showed only a 21.67 % decrease. After 14 days of accelerated aging, the Sn-58Bi solder experienced a significant reduction of 49.28 % in shear strength, whereas the solder with 1.00 wt.% activated BC displayed only a 31.14 % decrease. The enhanced shear strength of aged Sn-58Bi solder joints reinforced with activated BC nanoparticles can be attributed to BC's ability to regulate grain ripening, interfacial IMCs growth, and Kirkendall void formation.

Fracture surfaces transitioned from flat and smooth to elongated-dimple structures with the addition of activated BC. Prolonged accelerated aging led to an increased presence of cleavage due to the continuous formation of brittle Bi-rich layer, while higher amounts of activated BC decreased the number of facets and the size of voids, indicating effective suppression of Bi phase segregation and enhanced ductility.

Solder joints failed through three primary modes. Mode 1, the in-solder failure mode, was the preferred ductile fracture mode, while Mode 3, the IMC failure mode, represented an undesirable brittle fracture mode. The likelihood of Mode 1 failure increased with higher activated BC content and decreased with longer heat aging durations. Thus, 100 % Mode 1 failure was observed in the as-reflowed samples with 1.00 wt.% activated BC, while 100 % Mode 3 failure was observed in the pure Sn-58Bi samples after 14 days of heat aging.

Based on this study, the recommended composition for enhancing solder joint performance in PV modules was Sn-58Bi solder with the addition of 1.00 wt.% activated BC, as it demonstrated the highest shear strength, exhibited ductile fracture with a dimpled structure on the fracture surface, and failed in the desired Mode 1 failure mode.

CHAPTER 5

CONCLUSIONS AND RECOMMENDATIONS

5.1 Conclusions

In this study, changes in shear strengths of Sn-58Bi alloy containing varying amounts of a plant-based reinforcement, activated BC and the respective fracture behaviour and failure modes were investigated. The following conclusions can be drawn:

1. The shear strength of Sn-58Bi solder increased with higher activated BC content but decreased with longer heat-aging durations, with lower degradation rates observed with the addition of BC. Specifically, with 1.00 wt.% of activated BC, the shear strength of the as-reflowed solder joints increased by about 21.67 %. Additionally, the degradation in shear strength for the 14-day heat-aged specimens with 1.00 wt.% activated BC was 31.14 %, compared to 49.28 % for pure Sn-Bi solder. These findings indicated that the addition of 1.00 wt.% activated BC resulted in the highest shear strength for solder joints.
2. Sn-58Bi changed its fracture behaviour from brittle to more ductile, transitioning from a flat and smooth surface to elongated dimple structures with the addition of activated BC. While prolonged accelerated aging increased cleavage presence, more activated BC reduced cleavage facets and void size, indicating successful suppression of brittle Bi phase segregation and enhanced ductility. These findings indicated that all pure Sn-58Bi samples exhibited brittle fracture behaviour characterized by deep cleavage facets, whereas the reinforced samples exhibited shallow facets as the aging duration increased.
3. The IMC failure mode (Mode 3 – brittle fracture) exhibited the lowest solder strength, followed by the mixed solder/IMC failure mode (Mode 2 - combined ductile-brittle fracture) and the in-solder failure mode

(Mode 1 - ductile fracture). Mode 1 failure generally increased with higher activated BC content, while Mode 3 failure increased with longer heat treatment duration. These findings indicated that 100 % Mode 1 failure was observed in the as-reflowed samples with 1.00 wt.% activated BC, while 100 % Mode 3 failure was observed in the pure Sn-58Bi samples after 14 days of heat aging.

In conclusion, Sn-58Bi solder with 1.00 wt.% activated BC was identified as the recommended composition for enhancing metallization and connections in PV modules. The findings from this study demonstrated that activated BC is a viable reinforcement to address the inherent brittleness of Sn-58Bi solder, resulting in improved shear strength. Furthermore, it is not only low-cost but also sustainable and environmentally friendly, representing a significant step forward in reducing toxic Pb from PV waste.

5.2 Recommendations for future work

In this study, the effects of activated BC addition in Sn-58Bi solder with compositions ranging from 0.00 wt.% to 1.00 wt.% were investigated. The findings indicated that an increase in the amount of activated BC enhanced the shear strength of the solder and facilitated the Mode 1 ductile fracture behaviour. However, there may be a threshold level at which excessive amounts of activated BC content could be detrimental. Consequently, further research could be conducted to examine the effects of incorporating more than 1.00 wt.% of activated BC into Sn-58Bi solder.

Furthermore, recommendations for material testing are proposed. It is critical to assess solder joint strength in order to ensure the reliability and durability of electronic assemblies. The shear test was the only mechanical test performed in this project. In order to validate the effectiveness of activated BC in refining the microstructure, particularly in addressing the coarse Bi phase, suppressing excessive interfacial IMC growth, minimizing Kirkendall void formation, and regulating grain ripening during isothermal aging, it is necessary to conduct additional mechanical tests, such as tensile tests, drop tests, and fatigue tests, followed by fracture analysis.

Meanwhile, the sole thermal test that conducted was isothermal aging. Operational conditions and the service environment have a substantial impact on the long-term reliability and performance quality of electrical devices. Solder joints may experience a decrease in reliability as a result of the thermal stresses they endure during service. Thus, it is useful to conduct additional thermal tests, including thermal cycling, thermal shock, and thermal fatigue tests, to achieve a more comprehensive understanding.

Thermal cycling is a crucial test for determining the efficiency of PV modules as it evaluates the solder joint performance. This test is intended to evaluate the module's capacity to endure rapid temperature fluctuations between $-40\text{ }^{\circ}\text{C}$ and $85\text{ }^{\circ}\text{C}$. Such fluctuations exert stress on the module, revealing hidden defects such as poor soldering and delamination, caused by the differing thermal expansion coefficients of its components (SolarTec, 2015).

REFERENCES

- Aamir, M., Muhammad, R., Ahmed, N. and Waqas, M., 2017. Impact of thermal aging on the intermetallic compound particle size and mechanical properties of lead-free solder for green electronics. *Microelectronics Reliability*, [e-journal] 78, pp. 311–318. <https://doi.org/10.1016/j.microrel.2017.09.022>.
- Aamir, M., Muhammad, R., Tolouei-Rad, M., Giasin, K. and Silberschmidt, V. V., 2020. A review: microstructure and properties of tin-silver-copper lead-free solder series for the applications of electronics. *Soldering and Surface Mount Technology*, [e-journal] 32(2), pp. 115-126. <https://doi.org/10.1108/SSMT-11-2018-0046>.
- Abteu, M. and Selvaduray, G., 2000. Lead-free solders in microelectronics. *Materials Science and Engineering R: Reports*, [e-journal] 27(5), pp. 95-141. [https://doi.org/10.1016/S0927-796X\(00\)00010-3](https://doi.org/10.1016/S0927-796X(00)00010-3).
- An, T. and Qin, F., 2014. Effects of the intermetallic compound microstructure on the tensile behaviour of Sn3.0Ag0.5Cu/Cu solder joint under various strain rates. *Microelectronics Reliability*, [e-journal] 54(5), pp. 932-938. <https://doi.org/10.1016/j.microrel.2014.01.008>.
- ASTM International, 2019. *Standard Test Method for Apparent Shear Strength of Single-Lap-Joint Adhesively Bonded Metal Specimens by Tension Loading (Metal-to-Metal)*. [online] Available at: <<https://www.astm.org/d1002-10r19.html>> [Accessed 15 April 2024]
- Bara, J., 2020. *Common PCB Soldering Problems to Avoid*. [online] Available at: <<https://www.mwrf.com/materials/article/21126700/common-pcb-soldering-problems-to-avoid>> [Accessed 18 March 2023].
- Chantaramanee, S. and Sungkhaphaitoon, P., 2021. Influence of bismuth on microstructure, thermal properties, mechanical performance, and interfacial behaviour of SAC305-xBi/Cu solder joints. *Transactions of Nonferrous Metals Society of China (English Edition)*, [e-journal] 31(5), pp. 1397-1410. [https://doi.org/10.1016/S1003-6326\(21\)65585-1](https://doi.org/10.1016/S1003-6326(21)65585-1).
- Chan, F., 2023. *Exploring the Layers of a PCB: Composition and Structure Unveiled*. [online] Available at: <<https://www.linkedin.com/pulse/exploring-layers-pcb-composition-structure-unveiled-fiona-chan/>> [Accessed 18 March 2024].
- Chaturvedi, K., Singhwane, A., Dhangar, M., Mili, M., Gorhae, N., Naik, A., Prashant, N., Srivastava, A.K. and Verma, S., 2024. Bamboo for producing charcoal and biochar for versatile applications. *Biomass Conversion and Biorefinery*, [e-journal] 14, pp. 15159–15185. <https://doi.org/10.1007/s13399-022-03715-3>.

Chen, C., Zhang, L., Wang, X., Lu, X. and Guo, Y., 2023. Microstructure and properties of Sn58Bi/Ni solder joint modified by Mg particles. *Journal of Materials Research and Technology*, [e-journal] 24, pp. 514-526. <https://doi.org/10.1016/j.jmrt.2023.03.010>.

Chen, H.M., Liao, J., Wu, S., Gong, L., Wang, J. and Wang, H., 2018. Effects of Dy substitution for Sn on the solderability and mechanical property of the standard near eutectic Sn–Ag–Cu alloy. *Journal of Materials Science: Materials in Electronics*, [e-journal] 29(15), pp. 12662-12668. <https://doi.org/10.1007/s10854-018-9383-7>.

Chen, W.M., McCloskey, P. and O’Mathuna, S.C., 2006. Isothermal aging effects on the microstructure and solder bump shear strength of eutectic Sn37Pb and Sn3.5Ag solders. *Microelectronics Reliability*, [e-journal] 46(5), pp. 896-904. <https://doi.org/10.1016/j.microrel.2005.06.006>.

Cheng, S., Huang, C.M. and Pecht, M., 2017. A review of lead-free solders for electronics applications. *Microelectronics Reliability*, [e-journal] 75, pp. 77–95. <https://doi.org/10.1016/j.microrel.2017.06.016>.

ChipQuik, 2024. *Solder 42Sn/58Bi Solder Paste 250g Jar*. [online] Available at: <<https://my.mouser.com/ProductDetail/ChipQuik/SMDLTLFP250?qs=f4cZYvvsIBsU9w3hkBipI%3D%3D>> [Accessed 8 April 2024].

Choi, J.W. and Oh, T.S., 2001. *Shear strength and aging characteristics of Sn-Pb and Sn-Ag-Bi solder bumps*. In: Department of Metallurgical Engineering and Materials Science, 3rd International Symposium on Electronic Materials and Packaging. Jeju, Republic of Korea, 19-22 November 2001. New York: United Nations.

Dušek, K., Bušek, D., Veselý, P., Pražanová, A., Plaček, M. and Re, J. Del, 2022. Understanding the Effect of Reflow Profile on the Metallurgical Properties of Tin–Bismuth Solders. *Metals*, [e-journal] 12(1). <https://doi.org/10.3390/met12010121>.

Dušek, K. and Náhlík, V., 2012. *Comparison of commonly used fluxes aggression on copper surface*. In: Department of Electrotechnology, 35th International Spring Seminar on Electronics Technology. Bad Aussee, Austria, 9–13 May 2012. New York: United Nations.

Dušek, K., Veselý, P., Bušek, D., Petráč, A., Géczy, A., Illés, B. and Krammer, O., 2021. Influence of flux and related factors on intermetallic layer growth within SAC305 solder joints. *Materials*, [e-journal] 14(24). <https://doi.org/10.3390/ma14247909>.

- Gain, A.K. and Zhang, L., 2016a. Growth mechanism of intermetallic compound and mechanical properties of nickel (Ni) nanoparticle doped low melting temperature tin–bismuth (Sn–Bi) solder. *Journal of Materials Science: Materials in Electronics*, [e-journal] 27(1), pp. 781-794. <https://doi.org/10.1007/s10854-015-3817-2>.
- Gain, A.K. and Zhang, L., 2016b. Interfacial microstructure, wettability and material properties of nickel (Ni) nanoparticle doped tin–bismuth–silver (Sn–Bi–Ag) solder on copper (Cu) substrate. *Journal of Materials Science: Materials in Electronics*, [e-journal] 27(4), pp. 3982-3994. <https://doi.org/10.1007/s10854-015-4252-0>.
- Gain, A.K. and Zhang, L., 2016c. Microstructure, mechanical and electrical performances of zirconia nanoparticles-doped tin-silver-copper solder alloys. *Journal of Materials Science: Materials in Electronics*, [e-journal] 27(7), pp. 7524-7533. <https://doi.org/10.1007/s10854-016-4732-x>.
- Gain, A.K. and Zhang, L., 2017. Effect of Ag nanoparticles on microstructure, damping property and hardness of low melting point eutectic tin–bismuth solder. *Journal of Materials Science: Materials in Electronics*, [e-journal] 28(20), pp. 15718-15730. <https://doi.org/10.1007/s10854-017-7465-6>.
- Gao, Y., Bian, X., Qiu, X., Jia, Y., Yi, J. and Wang, G., 2023. Investigation of Microstructure and Mechanical Properties of SAC105 Solders with Sb, In, Ni, and Bi Additions. *Materials*, [e-journal] 16(11). <https://doi.org/10.3390/ma16114059>.
- Görlich, J., Oberdorfer, C., Baither, D., Schmitz, G., Reinke, C. and Wilke, U., 2010. The role of oxide layers in solder joints. *Journal of Alloys and Compounds*, [e-journal] 490(1–2), pp. 336-341. <https://doi.org/10.1016/j.jallcom.2009.10.005>.
- Guo, J., Zhao, X., Liu, Y., Tan, C., Liu, L., Ning, X., Nie, Z. and Yu, X., 2020. The effect of Ag on the growth of intermetallic at the interface of Sn5Zn/Cu interconnects. *Materials Today Communications*, [e-journal] 24. <https://doi.org/10.1016/j.mtcomm.2020.100960>.
- Han, B., Sun, F., Ban, G., Liu, Y., Li, T. and Pang, S., 2019. Effect of Cu, Ag on the microstructure and IMC evolution of Sn5Sb-CuAgNi/Cu solder joints. *Materials Research Express*, [e-journal] 6(8). <https://doi.org/10.1088/2053-1591/ab1f4a>.
- Ho, C.E., Yang, S.C. and Kao, C.R., 2007. Interfacial reaction issues for lead-free electronic solders. *Journal of Materials Science: Materials in Electronics*, [e-journal] 18(1–3), pp. 155-174. <https://doi.org/10.1007/s10854-006-9031-5>.
- Hu, F.Q., Zhang, Q.K., Jiang, J.J. and Song, Z.L., 2018. Influences of Ag addition to Sn-58Bi solder on SnBi/Cu interfacial reaction. *Materials Letters*, [e-journal] 214, pp. 142-145. <https://doi.org/10.1016/j.matlet.2017.11.127>.

Hu, T., Li, Y., Chan, Y.C. and Wu, F., 2015. Effect of nano Al₂O₃ particles doping on electromigration and mechanical properties of Sn-58Bi solder joints. *Microelectronics Reliability*, [e-journal] 55(8), pp. 1226-1233. <https://doi.org/10.1016/j.microrel.2015.05.008>.

Illés, B., Krammer, O. and Géczy, A., 2020. *Introduction to surface-mount technology*, pp. 1-62.

Isa, S.S.M., Ramli, M.M., Hambali, N.A.M.A., Kasjoo, S.R., Isa, M.M., Nor, N.I.M., Khalid, N. and Ahmad, N., 2016. Adsorption Properties and Potential Applications of Bamboo Charcoal: A Review. *MATEC Web of Conferences*, 78, p. 1097.

Izwan, M.I., Saud, N., Salleh, M.A.A., Derman, M.N., Said, R.M. and Nasir, N., 2015. Influence of Micron-Size Activated Carbon Additions on the Microstructure, Microhardness and Thermal Properties of Sn-Cu-Ni (SN100C) Solder Fabricated via Powder Metallurgy Method. *Applied Mechanics and Materials*, [e-journal] 754–755, pp. 513-517. <https://doi.org/10.4028/www.scientific.net/amm.754-755.513>.

Jiang, N., Zhang, L., Liu, Z.Q., Sun, L., Long, W.M., He, P., Xiong, M.Y. and Zhao, M., 2019. Reliability issues of lead-free solder joints in electronic devices. *Science and Technology of Advanced Materials*, [e-journal] 20(1), pp. 876–901. <https://doi.org/10.1080/14686996.2019.1640072>.

Jiang, Y., He, Y. and Liu, C.T., 2018. Review of porous intermetallic compounds by reactive synthesis of elemental powders. *Intermetallic*, [e-journal] 93, pp. 217–226. <https://doi.org/10.1016/j.intermet.2017.06.003>.

Kang, H., Rajendran, S.H. and Jung, J.P., 2021. Low melting temperature Sn-Bi solder: Effect of alloying and nanoparticle addition on the microstructural, thermal, interfacial bonding, and mechanical characteristics. *Metals*, [e-journal] 11(2). <https://doi.org/10.3390/met11020364>.

Kaya, M. ed., 2019. *Printed Circuit Boards (PCBs)*. Switzerland: Springer.

Koji, Y., 2019. High aspect ratio solder printing technology enabling mixed mounting from 0402M components to large components. *Omron Technics*, 51(1), pp. 1-7.

Kumar, N. and Maurya, A., 2022. Development of lead-free solder for electronic components based on thermal analysis. *Materials Today: Proceedings*, [e-journal] 62(4), pp. 2163–2167. <https://doi.org/10.1016/j.matpr.2022.03.358>.

Kurtz, S., Whitfield, K., Miller, D., Joyce, J., Wohlgemuth, J., Kempe, M., Dhere, N., Bosco, N. and Zgonena, T., 2009. *Evaluation of high-temperature exposure of rack-mounted photovoltaic modules*. In: National, Renewable Energy Laboratory, 34th IEEE Photovoltaic Specialists Conference. Philadelphia, Pennsylvania, 7–12 June 2009. New York: United Nations.

Li, Z., Wu, G., Ding, K. and Gao, Y., 2022. Role of the Aging Treatment in the Microstructure Evolution and Mechanical Properties of Cu/Sn-Bi-Ag-In/Cu Joint. *Minerals, Metals and Materials Series*, [e-journal] 151, pp. 1079–1087. https://doi.org/10.1007/978-3-030-92381-5_103.

Liu, L., Xue, S. and Liu, S., 2018. Mechanical property of Sn-58Bi solder paste strengthened by resin. *Applied Sciences (Switzerland)*, [e-journal] 8(11). <https://doi.org/10.3390/app8112024>.

Liu, X., Huang, M., Wu, C. M. L., and Wang, L., 2010. Effect of YO particles on microstructure formation and shear properties of Sn-58Bi solder. *Journal of Materials Science: Materials in Electronics*, 21(10), pp. 1046 – 1054.

Liu, Y., Sun, F., Zhang, H. and Zou, P., 2012. Solderability, IMC evolution, and shear behaviour of low-Ag Sn_{0.7}Ag_{0.5}Cu-BiNi/Cu solder joint. *Journal of Materials Science: Materials in Electronics*, [e-journal] 23(9), pp. 1705–1710. <https://doi.org/10.1007/s10854-012-0649-1>.

Liu, Y. and Tu, K.N., 2020. Low melting point solders based on Sn, Bi, and In elements. *Materials Today Advances*, [e-journal] 8. <https://doi.org/10.1016/j.mtadv.2020.100115>.

Lu, X., Zhang, L., Chen, C. and Wang, X., 2023. Microstructure and orientation evolution of β -Sn and interfacial Cu₆Sn₅ IMC grains in SAC105 solder joints modified by Si₃N₄ nanowires. *Journal of Materials Research and Technology*, [e-journal] 26, pp. 4723–4738. <https://doi.org/10.1016/j.jmrt.2023.08.186>.

Ma, H. and Suhling, J.C., 2009. A review of mechanical properties of lead-free solders for electronic packaging. *Journal of Materials Science*, [e-journal] 44, pp. 1141–1158. <https://doi.org/10.1007/s10853-008-3125-9>.

Ma, H., Zhao, B., Wu, G., Li, Z. and Gao, Y., 2021. A SnBiAgIn solder alloy with exceptional mechanical properties by rapid quenching. *Journal of Materials Science: Materials in Electronics*, [e-journal] 32(6), pp. 8167–8173. <https://doi.org/10.1007/s10854-021-05539-9>.

Mohd Salleh, M.A.A., Bakri, A.M.M. Al, Zan Hazizi, M.H., Somidin, F., Mohd Alui, N.F. and Ahmad, Z.A., 2012. Mechanical properties of Sn-0.7Cu/Si₃N₄ lead-free composite solder. *Materials Science and Engineering: A*, [e-journal] 556, pp. 633–637. <https://doi.org/10.1016/j.msea.2012.07.039>.

Mokhtari, O. and Nishikawa, H., 2013. *Coarsening of Bi phase and intermetallic layer thickness in Sn-58Bi-X (X=In and Ni) solder joint*. In: Joining and Welding Research Institute, 14th International Conference on Electronic Packaging Technology. Dalian, China, 11–14 August 2013. York: United Nations.

- Mokhtari, O. and Nishikawa, H., 2016. Correlation between microstructure and mechanical properties of Sn-Bi-X solders. *Materials Science and Engineering: A*, [e-journal] 651, pp. 831-839. <https://doi.org/10.1016/j.msea.2015.11.038>.
- Mookam, N. and Kanlayasiri, K., 2018. Influences of soldering time on wettability and intermetallic phase between Sn-3.0Cu solder and copper substrate. *MATEC Web of Conferences*, 192(1024), pp. 1-4.
- Padoan, F.C.S.M., Altimari, P. and Pagnanelli, F., 2019. Recycling of end-of-life photovoltaic panels: A chemical prospective on process development. *Solar Energy*, [e-journal] 177, pp. 746–761. <https://doi.org/10.1016/j.solener.2018.12.003>.
- Palaniappan, S.C.K. and Martin.K.A. ed., 2016. *A study on process, strength and microstructure analysis*. USA: Rochester Institute of Technology.
- Pan, J., Toleno, B.J., Chou, T.C. and Dee, W.J., 2006. The effect of reflow profile on SnPb and SnAgCu solder joint shear strength. *Soldering and Surface Mount Technology*, 18(4). <https://doi.org/10.1108/09540910610717901>.
- Peng, W., 2009. An investigation of Sn pest in pure Sn and Sn-based solders. *Microelectronics Reliability*, [e-journal] 49(1), pp. 86-91. <https://doi.org/10.1016/j.microrel.2008.11.001>.
- Peng, W., Monlevade, E. and Marques, M.E., 2007. Effect of thermal aging on the interfacial structure of SnAgCu solder joints on Cu. *Microelectronics Reliability*, [e-journal] 47(12), pp. 2161-2168. <https://doi.org/10.1016/j.microrel.2006.12.006>.
- Perdigones, F. and Quero, J.M., 2022. Printed Circuit Boards: The Layers' Functions for Electronic and Biomedical Engineering. *Micromachines*, [e-journal] 13(3). <https://doi.org/10.3390/mi13030460>.
- Peterson, Z., 2024. *What is a PCB and Intro to PCB Design*. [online] Available at: <<https://resources.altium.com/p/what-is-a-pcb>> [Accessed 18 March 2024].
- Rajendran, S.H., Hwang, S.J. and Jung, J.P., 2020. Shear strength and aging characteristics of Sn-3.0Ag-0.5Cu/Cu solder joint reinforced with ZrO₂ nanoparticles. *Metals*, [e-journal] 10(10). <https://doi.org/10.3390/met10101295>.
- Rajendran, S.H., Kang, H. and Jung, J.P., 2021. Ultrasonic-Assisted Dispersion of ZnO Nanoparticles to Sn-Bi Solder: A Study on Microstructure, Spreading, and Mechanical Properties. *Journal of Materials Engineering and Performance*, [e-journal] 30(5), pp. 3167-3172. <https://doi.org/10.1007/s11665-021-05518-5>.

Ramli, M.I.I., Mohd Salleh, M.A.A., Derman, M.N., Said, R.M. and Saud, N., 2016. Influence of Activated Carbon Particles on Intermetallic Compound Growth Mechanism in Sn-Cu-Ni Composite Solder. *MATEC Web of Conferences*, 78 (1064), pp. 1–7.

Said, R.M., Saud, N., Mohd Salleh, M.A.A., Derman, M.N., Izwan Ramli, M.I. and Nasir, N.M., 2015. The Influence of Activated Carbon (AC) on Melting Temperature, Wettability and Intermetallic Compound Formation of Sn-Cu-Ni (SN100C) Solder Paste. *Applied Mechanics and Materials*, [e-journal] 754–755, pp. 551-555. <https://doi.org/10.4028/www.scientific.net/amm.754-755.551>.

Sayyadi, R. and Naffakh-Moosavy, H., 2019. The Role of Intermetallic Compounds in Controlling the Microstructural, Physical and Mechanical Properties of Cu-[Sn-Ag-Cu-Bi]-Cu Solder Joints. *Scientific Reports*, [e-journal] 9(1). <https://doi.org/10.1038/s41598-019-44758-3>.

Sayyidah A.M. ed., 2015. *Development of Sn-Cu Filled Activated Carbon Composite Solder via Powder Metallurgy Technique*. Perlis: University Malaysia Perlis.

Sharma, K., Sharma, V. and Sharma, S.S., 2018. Dye-Sensitized Solar Cells: Fundamentals and Current Status. *Nanoscale Research Letters*, [e-journal] 13(381). <https://doi.org/10.1186/s11671-018-2760-6>.

Silva, B.L., Xavier, M.G.C., Garcia, A. and Spinelli, J.E., 2017. Cu and Ag additions affecting the solidification microstructure and tensile properties of Sn-Bi lead-free solder alloys. *Materials Science and Engineering: A*, [e-journal] 705, pp. 325-334. <https://doi.org/10.1016/j.msea.2017.08.059>.

Singh, A., Durairaj, R., Chian, L.K., Noor, E.E.M. and Yoong, S.Y., 2018. Reliability study of lead-free Sn-3.8Ag-0.7Cu and copper (Cu) substrate based on the microstructure, physical and mechanical properties. *Journal of Mechanical Engineering*, 5(2), pp. 169-180.

Singh, A., Khai, T.S., Durairaj, R. and Saleh, A.A.Q., 2022. Preliminary Investigation of Copper Joints Soldered with Sn58Bi. *Journal of Harbin Institute of Technology (New Series)*, [e-journal] 29(1), pp. 57-63. <https://doi.org/10.11916/j.issn.1005-9113.2020040>.

Siti Rabiattull Aisha, I., Ourdjini, A., Azmah Hanim, M.A. and Saliza Azlina, O., 2015. Effect of reflow soldering profile on intermetallic compound formation. *International Journal of Computer Applications in Technology*, [e-journal] 52(4). <https://doi.org/10.1504/IJCAT.2015.073590>.

SolarTec, 2015. *Diagnose and Test Laboratory of PV modules*. [online] Available at:

<<https://mymouser.com/ProductDetail/ChipQuik/SMDLTLFP250?qs=f4cZYvvs1BsU9w3hkBipIg%3D%3D>> [Accessed 6 October 2024].

Song, Q., Yang, W., Li, Y., Mao, J., Qin, W. and Zhan, Y., 2021. Interfacial reaction and mechanical properties of Sn58Bi-XCr solder joints under isothermal aging conditions. *Vacuum*, [e-journal] 194. <https://doi.org/10.1016/j.vacuum.2021.110559>.

Subyakto, S., Budiman, I. and Pari, G., 2017. Effects of Temperature and Time of Carbonization on the Properties of Bamboo (*Dendrocalamus asper*) Carbon. *Wood Research Journal*, [e-journal] 4(1). <https://doi.org/10.51850/wrj.2012.3.2.68-73>.

Thao, D.N., 2023. *The Differences Between Bamboo Charcoal Powder Vs Activated Charcoal*. [online] Available at: <<https://vietnamcharcoal.com/bamboo-charcoal-powder-vs-activated-charcoal/>> [Accessed 5 April 2024]

Ting Tan, A., Wen Tan, A. and Yusof, F., 2015. Influence of nanoparticle addition on the formation and growth of intermetallic compounds (IMCs) in Cu/Sn-Ag-Cu/Cu solder joint during different thermal conditions. *Science and Technology of Advanced Materials*, [e-journal] 16. <https://doi.org/10.1088/1468-6996/16/3/033505>.

Tsai, T.N., 2005. Development of an integrated reflow soldering control system using incremental hybrid process knowledge. *Expert Systems with Applications*, [e-journal] 28(4), pp. 681-692. <https://doi.org/10.1016/j.eswa.2004.12.025>.

Vianco, P.T., 1993. *Development of alternatives to lead-bearing solders*. In: Sandia National Labs, Surface Mount Technical Association International Conference. San Jose, United States, 31 August – 2 September 1993. New York: United Nations

Wang, F., Huang, Y., Zhang, Z. and Yan, C., 2017a. Interfacial reaction and mechanical properties of Sn-Bi solder joints. *Materials*, [e-journal] 10(8). <https://doi.org/10.3390/ma10080920>.

Wang, F., Li, D., Zhang, Z., Wu, M. and Yan, C., 2017b. Improvement on interfacial structure and properties of Sn–58Bi/Cu joint using Sn–3.0Ag–0.5Cu solder as barrier. *Journal of Materials Science: Materials in Electronics*, [e-journal] 28(24), pp. 19051-19060. <https://doi.org/10.1007/s10854-017-7859-5>.

Wang, J., Ashworth, M.A. and Wilcox, G.D., 2014. An investigation into the role of lead as a suppressant for tin whisker growth in electronics. *IEEE Transactions on Components, Packaging and Manufacturing Technology*, [e-journal] 4(4), pp. 727-740. <https://doi.org/10.1109/TCPMT.2014.2302802>.

Wang, J., Wei, H., He, P., Lin, T. and Lu, F., 2015. Microstructure and Mechanical Properties of Tin-Bismuth Solder Reinforced by Aluminium Borate Whiskers. *Journal of Electronic Materials*, [e-journal] 44(10), pp. 3872-3879. <https://doi.org/10.1007/s11664-015-3896-0>.

Wang, K., Wang, F., Huang, Y. and Qi, K., 2019a. Comprehensive properties of a novel quaternary Sn-Bi-Sb-Ag solder: Wettability, interfacial structure and mechanical properties. *Metals*, [e-journal] 9(7).
<https://doi.org/10.3390/met9070791>.

Wang, X., Zhang, L., Li, M. Ian, Wang, X. and Zhao, M., 2022. Enhancement of structure and properties of Sn58Bi solder by AlN ceramic particles. *Journal of Materials Research and Technology*, [e-journal] 19, pp. 2584-2595.
<https://doi.org/10.1016/j.jmrt.2022.06.001>.

Wang, Z., Zhang, Q.K., Chen, Y.X. and Song, Z.L., 2019b. Influences of Ag and In alloying on Sn-Bi eutectic solder and SnBi/Cu solder joints. *Journal of Materials Science: Materials in Electronics*, [e-journal] 30(20), pp. 18524-18538. <https://doi.org/10.1007/s10854-019-02206-y>.

Waseem, U., 2023. *Solder Reflow: An In-Depth Guide to the Process and Techniques*. [online] Available at: <<https://www.wevolver.com/article/solder-reflow-an-in-depth-guide-to-the-process-and-techniques>> [Accessed 19 March 2024].

Weaver, J., 2022. World has installed 1TW of solar capacity – pv magazine International. *PV Magazine*, [online] 15 March. Available at: <<https://www.pv-magazine.com/2022/03/15/humans-have-installed-1-terawatt-of-solar-capacity/>> [Accessed 7 August 2024].

Weckend, S., Wade, A. and Heath, G., 2016. *End of Life Management Solar PV Panels*. Germany: International Renewable Energy Agency (IRENA) and the International Energy Agency (IEA).

Weinberg, K. and Böhme, T., 2009. Condensation and growth of Kirkendall voids in intermetallic compounds. *IEEE Transactions on Components and Packaging Technologies*, [e-journal] 32(3), pp. 684-692.
<https://doi.org/10.1109/TCAPT.2008.2010057>.

Whalley, D.C., 2004. A simplified reflow soldering process model. *Journal of Materials Processing Technology*, [e-journal] 150 (1-2), pp. 134-144.
<https://doi.org/10.1016/j.jmatprotec.2004.01.029>.

Yang, F., Zhang, L., Liu, Z.Q., Zhong, S.J., Ma, J. and Bao, L., 2016. Properties and Microstructures of Sn-Bi-X Lead-Free Solders. *Advances in Materials, Science and Engineering*, [e-journal] 1-15,
<https://doi.org/10.1155/2016/9265195>.

Yang, L., Du, C., Dai, J., Zhang, N. and Jing, Y., 2013. Effect of nanosized graphite on properties of Sn-Bi solder. *Journal of Materials Science: Materials in Electronics*, [e-journal] 24(11), pp. 4180-4185.
<https://doi.org/10.1007/s10854-013-1380-2>.

Yang, L., Zhou, S., Zhang, Y., Zhu, L., Xiong, Y., Jiang, W. and Shen, S., 2019. Reinforcement of vanadium on the microstructure and properties of Sn-58Bi lead-free solder joints. *Materials Research Express*, [e-journal] 6(6). <https://doi.org/10.1088/2053-1591/ab07f6>.

Yang, T., Chen, Y., You, K., Dong, Z., Jia, Y., Wang, G., Peng, J., Cai, S., Luo, X., Liu, C. and Wang, J., 2022. Effect of Bi, Sb, and Ti on Microstructure and Mechanical Properties of SAC105 Alloys. *Materials*, [e-journal] 15(14). <https://doi.org/10.3390/ma15144727>.

Yang, T., Zhao, X., Xiong, Z., Tan, W., Wei, Y., Tan, C., Yu, X. and Wang, Y., 2020. Improvement of microstructure and tensile properties of Sn–Bi–Ag alloy by heterogeneous nucleation of β -Sn on Ag₃Sn. *Materials Science and Engineering: A*, [e-journal] 785. <https://doi.org/10.1016/j.msea.2020.139372>.

Yee, S.C., Wong, K.M.C. and Issabayeva, G., 2019. *A Study on the Shear Strength and Failure Modes of Sn-3.0Ag-0.5Cu Solder Joint Containing Pt*. In: Department of Mechanical and Materials Engineering, IOP Conference Series: Materials Science and Engineering. Sarawak, Malaysia, 26–28 November 2018. England, UK.

Yeh, C.H., Chang, L.S. and Straumal, B.B., 2011. Wetting transition of grain boundaries in the Sn-rich part of the Sn–Bi phase diagram. *Journal of Materials Science*, [e-journal] 46(5), pp. 1557–1562. <https://doi.org/10.1007/s10853-010-4961-y>.

Yim, Y.J. and Kim, B.J., 2023. Preparation and Characterization of Activated Carbon/Polymer Composites: A Review. *Polymers*, [e-journal] 15(16). <https://doi.org/10.3390/polym15163472>.

Yoon, J.W., Lee, C.B. and Jung, S.B., 2002. Interfacial reactions between Sn-58 mass% Bi eutectic solder and (Cu, electroless Ni-P/Cu) substrate. *Materials Transactions*, [e-journal] 43(8), pp. 1821–1826. <https://doi.org/10.2320/matertrans.43.1821>.

Zeng, K. and Tu, K.N., 2002. Six cases of reliability study of Pb-free solder joints in electronic packaging technology. *Materials Science and Engineering: R: Reports*, [e-journal] 38(2), pp. 55–105. [https://doi.org/10.1016/s0927-796x\(02\)00007-4](https://doi.org/10.1016/s0927-796x(02)00007-4).

Zhai, X., Chen, Y., Li, Y., Zou, J., Shi, M., Yang, B., Guo, C., Hu, R. and Su, X., 2021. Research on the Mechanical and Performance Effects of Flux on Solder Layer Interface Voids. *Journal of Electronic Materials*, [e-journal] 50(12), pp. 6629–6638. <https://doi.org/10.1007/s11664-021-09157-3>.

Zhang, H., Sun, F. and Liu, Y., 2019. Copper foam enhanced Sn58Bi solder joint with high performance for low temperature packaging. *Materials Letters*, [e-journal] 241, pp. 108–110. <https://doi.org/10.1016/j.matlet.2019.01.056>.

Zhang, L., Yang, W., Feng, J., Qin, W., Qi, D., Song, S. and Zhan, Y., 2023. Effect of the addition of CeO₂ nanoparticles on the microstructure and shear properties of Sn–57Bi–1Ag solder alloy. *Journal of Materials Research and Technology*, [e-journal] 26, pp. 1062-1078.
<https://doi.org/10.1016/j.jmrt.2023.07.260>.

Zhang, P., Xue, S., Liu, L., Wu, J., Luo, Q. and Wang, J., 2022. Microstructure and Shear Behaviour of Sn-3.0Ag-0.5Cu Composite Solder Pastes Enhanced by Epoxy Resin. *Polymers*, [e-journal] 14(23).
<https://doi.org/10.3390/polym14235303>.

Zhang, P., Xue, S., Wang, J., Xue, P., Zhong, S. and Long, W., 2019. Effect of nanoparticles addition on the microstructure and properties of lead-free solders: A review. *Applied Sciences (Switzerland)*, [e-journal] 9(10).
<https://doi.org/10.3390/app9102044>.

Zhang, Q.K., Zou, H.F. and Zhang, Z.F., 2011. Influences of substrate alloying and reflow temperature on bi segregation behaviours at Sn-Bi/Cu interface. *Journal of Electronic Materials*, [e-journal] 40(11), pp. 2320-2328.
<https://doi.org/10.1007/s11664-011-1742-6>.

Zhong, S., Zhang, L., Li, M., Long, W. and Wang, F., 2022. Development of lead-free interconnection materials in electronic industry during the past decades: Structure and properties. *Materials and Design*, [e-journal] 215.
<https://doi.org/10.1016/j.matdes.2022.110439>.

Zhou, Z., Ma, X., Zhou, M.B., Yin, C. and Zhang, X.P., 2017. *Effect of isothermal aging on mechanical properties and strain rate sensitivity of the eutectic Sn-58Bi solder alloy*. In: Lab of Smart Materials and Electronic Packaging in School of Materials Science and Engineering, 18th International Conference on Electronic Packaging Technology. Harbin, China, 16–19 August 2017. New York: United Nations.

Zuberbuehler, T., 2021. *What Is Soldering Flux?* [online] Available at: <<https://versae.com/what-is-a-soldering-flux/>> [Accessed 19 March 2024]

APPENDICES

Appendix A: Figure

10/1/24, 12:33 PM

Universiti Tunku Abdul Rahman Mail - IConGEET2024: Official Invoice and Acceptance Letter (IConGEET2024: 073-061)



Dr Karen Wong Mee Chu <mcwong@utar.edu.my>

IConGEET2024: Official Invoice and Acceptance Letter (IConGEET2024: 073-061)

1 message

IConGEET International Conference <icongeet@unimap.edu.my>
 To: "mcwong@utar.edu.my" <mcwong@utar.edu.my>

Fri, Sep 27, 2024 at 10:56 AM

Dear Participant,

We hope this email finds you well.

We are pleased to inform you that your paper titled " Fracture behaviour of Sn-58Bi alloy reinforced by activated bamboo charcoal " has been accepted for publication in E3S Web of Conferences a Scopus indexed proceedings for the 6th International Conference on Green Environmental Engineering and Technology (IConGEET2024).

Please find attached the following documents:

1. Invoice and Acceptance Letter
2. Reviewer comments
3. Copyright form

We kindly request that you proceed with the payment as per the invoice instructions at your earliest convenience. Please ensure that the payment is completed before submitting your camera-ready manuscript, as failure to do so may affect the consideration of your paper for publication.

Should you have any questions or require further assistance, feel free to contact us at icongeet@unimap.edu.my.

Thank you for your participation and support. We look forward to your contribution to IConGEET2024.

Best regards,

IConGEET2024 Publication Team

4 attachments

-  publication_right_form.pdf
441K
-  IConGEET2024_073-061.pdf
563K
-  Review_IConGEET2024_073_061_1.pdf
27K
-  Review_IConGEET2024_073_061.pdf
1429K

<https://mail.google.com/mail/u/0/?ik=d4bdf97e8e&view=pt&search=all&permthid=thread-f:1811316246210168113&simpl=msg-f:18113162462101...> 1/1

Figure A.1: Publication in ICONGEET 2024

¹Fracture behaviour of Sn-58Bi alloy reinforced by activated bamboo charcoal

Karen Mee Chu Wong^{1}, Jing Yee Chai¹, Muhammad Mahyiddin Ramli², Boon Han Lim³ and Siew Hoong Shuit⁴*

¹ Department of Mechanical and Materials Engineering, Lee Kong Chian Faculty of Engineering and Science, Universiti Tunku Abdul Rahman (UTAR), Bandar Sungai Long, Selangor, Malaysia

² Institute of Nano Electronic Engineering (INEE), Universiti Malaysia Perlis (UniMAP), Arau, Perlis, Malaysia
Faculty of Electronic Engineering and Technology, Universiti Malaysia Perlis (UniMAP), Arau, Perlis, Malaysia

³ Department of Electrical and Electronics Engineering, Lee Kong Chian Faculty of Engineering and Science, Universiti Tunku Abdul Rahman (UTAR), Bandar Sungai Long, Selangor, Malaysia

⁴ Department of Chemical Engineering, Lee Kong Chian Faculty of Engineering and Science, Universiti Tunku Abdul Rahman (UTAR), Bandar Sungai Long, Selangor, Malaysia

Abstract. Sn-Bi solders are considered by PV manufacturers as acceptable Pb-free alternative due to its low operating temperature and cost, despite being prone to brittleness caused by coarse Bi phases. Bamboo charcoal (BC) is a sustainable and environment-friendly resource with high surface area and its addition to Sn-Bi solder meets the requirement of a green solder, in line with environmental regulations. This study aims to improve the shear strength and reduce brittleness of the Sn-Bi solder alloy by using a sustainable reinforcement, the activated bamboo charcoal. Sn-58Bi solder paste was reinforced with 0.25, 0.50, 0.75 and 1.00 wt.% of activated BC, respectively and reflowed to create a single lap shear joint. Aging response was determined through accelerated aging at 120 °C for 7 days and 14 days. Shear strength of the joints increased as the activated BC content increased in the as-reflowed condition and there was lower degradation in shear strength for heat-aging specimens compared to pure Sn-Bi solder. No failures occurred via Mode 3 when the as-reflowed samples contained 0.50 wt.% or more of activated BC, and the 7- and 14-day heat-aged samples were free from Mode 3 failures when the activated BC composition was at 0.75 wt.% and above. Fracture surfaces showed transitions from flat and smooth surface to elongated-dimple structures even with just 0.25 wt.% of activated BC addition. While prolonged heat-aging increased cleavage presence, increasing amounts of activated BC reduced facet numbers and dimple sizes, indicating successful suppression of Bi phase segregation.

¹ Corresponding author: mcwong@utar.edu.my

1. Introduction

Solar industry has expanded rapidly and is expected to continue to rise due to increased energy demand amidst the transition towards net-zero. Increased installation of photovoltaic modules (PV) results in huge volume of PV waste as solar panels have limited lifespan of 25-30 years [1]. The estimated 60-78 million tonnes of PV waste by 2050 [2] includes the alarmingly toxic Pb pose new challenge. Pb-containing solders are used in the metallization and connections of the PV modules. Presently, restriction on use of Pb is being discussed at different regulatory levels [3]. Bi-containing solders are considered by PV manufactures [4] as Pb-free replacement due to its low operating temperature and low cost, albeit inferior properties, such as brittleness due to coarsened Bi-phase [5, 6]. It meets the requirement of a green solder, and its low operating temperature will not require complete overhaul of the existing manufacturing line. Research on Sn-Bi, the low-temperature alternative solder alloy for PV applications is still ongoing [7]. Common methods to improve performance of Bi-containing solders include addition of alloying elements [8–12], reinforcement [13] and heat-treatments [14,15]

Bamboo charcoal (BC) is made up from pieces of bamboo which undergoes a heat treatment normally between 800-1200°C. The carbonization process of this material will produce an enormous surface area-to-mass ratio which has high ability to attract and hold a wide range of materials, chemicals, radio waves, humidity, odours and harmful substances. By varying the temperature of carbonization, this material can be transformed from insulator to semiconductor and even to conductor as the pore size increases [16]. Addition of activated carbon to Sn-Cu-Ni solder resulted in thinner intermetallic (IMC) layer and increased shear strength of the solder joint [17]. As an alternative to activated carbon, carbon nanotubes, graphene and other carbon-based materials, it is the most notable among readily and renewable biomass resources because bamboo is the fastest growing plants in Earth and can expand by at least 60cm daily [18] and is low in cost. Due to the inherently large specific surface area and abundant pores, this environmentally friendly and sustainable plant-based reinforcement is expected to achieve maximum contact with the Bi-phase to suppress the coarsening and thus reduce brittleness. In this study, the fracture behaviour and failure modes of Sn-58Bi solder alloy reinforced by varying weight percentages of BC is investigated.

2. Materials & method

Commercial Sn-58Bi solder paste from ChipQuik with average particle diameter of 25 - 45 μm was used while the reinforcement was activated BC supplied by Future Food. Sn-58Bi-xBC composite solder samples were created by incorporating varying wt.% of activated BC into the Sn-58Bi solder paste, where x represented 0.00, 0.25, 0.50, 0.75, and 1.00 wt.%, respectively. The mixture was mechanically stirred to ensure homogeneity. A blank printed circuit board (PCB), referred to as a Cu substrate, was cleaned with ethanol and distilled water after being sectioned into dimensions of 50 mm x 10 mm x 1.5 mm. A stencil with an aperture area of 10 x 10 mm² and a thickness of 0.2 mm was positioned on the PCB piece, enabling precise and consistent screen printing of the composite solder sample at the designated location. After removing the stencil, another PCB piece was stacked on top to form a single lap shear joint specimen. Reflow was carried out in a programmable furnace, starting with preheating from 25 °C to 138 °C for 210 seconds, followed by a peak temperature of 165 °C for 30 seconds. Samples were then cooled to 138 °C and then to room temperature. Samples for accelerated aging were heat-treated at 120 °C for 7 and 14 days.

Shear strength of solder joints were determined using Shimadzu Autograph AGS-X Series Universal testing machine in accordance with ASTM D1002 with a crosshead speed of 1.2 mm/min. A minimum of 3 samples were tested for each condition. The fractured surfaces of Cu/Sn-58Bi-xBC/Cu solder joints were sectioned into 10 x 10 mm² samples and examined using a Hitachi S-3400 N scanning electron microscope (SEM) equipped with Energy-dispersive X-ray (EDX). SE mode with an accelerating voltage of 15kV and magnification of 750X was used.

3. Results & discussion

Figure 1 shows the shear strengths for Sn-58Bi alloy reinforced by varying amounts of activated BC content. In the as-reflowed condition, the shear strength of the Sn-58Bi alloy was 46 MPa and increased by 4.9%, 14.32%, 15.67% and 21.67% when 0.25wt.%, 0.50wt.%, 0.75wt.% and 1.00 wt.% of activated BC was added. Samples that were heat-treated at 120 °C for 7 and 14 days, respectively, exhibited increased shear strength with increasing amounts of activated BC additions. The porous nature and huge specific surface area of activated BC enhance its adsorption capabilities, allowing it to establish extensive contact with the coarse Bi-phase in the solder [16]. This will suppress the coarsening of the solder microstructure, which can cause brittleness. Solder microstructural refinement was proportional to the weight percentage of activated BC, leading to a more homogeneous distribution of phases within the solder, which in turn, improved the shear strength.

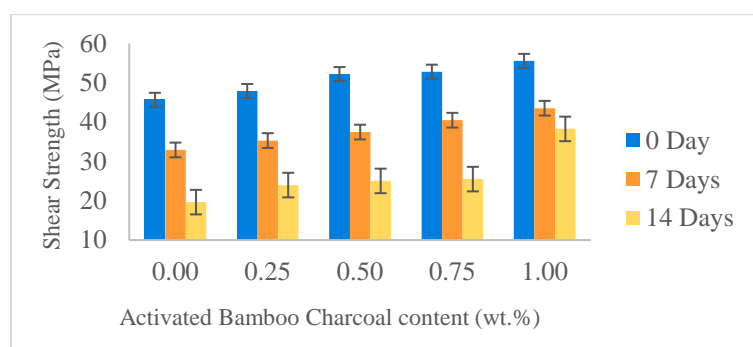


Fig.1. Shear test results for Sn-58Bi alloy with varying amounts of activated bamboo charcoal content.

After isothermal aging at 120 °C, the shear strength of both pure and reinforced Sn-58Bi solders decreased as the duration of heat treatment increased. However, the decline in shear strength was more significant in solder joints without activated BC. After 14 days of aging, the Sn-58Bi solder exhibited a substantial 57 % decrease in shear strength, whereas the solder containing 1.00 wt.% activated BC exhibited only a 32 % decrease. These variances indicate that the reliability of Sn-58Bi solder could be improved in high-temperature environments by incorporating activated BC nanoparticles. During solid-state diffusion, the activated BC's ability to control grain ripening, interfacial IMC growth, and Kirkendall void formation was responsible for the enhanced shear strength of aged Sn-58Bi solder joints with activated BC reinforcement [19,20]. Activated BC possibly prevented segregation of Bi precipitates by providing heterogeneous nucleation sites. Additionally, it may be adsorbed at the IMC layer, which reduced Kirkendall voids by inhibiting excessive interfacial growth that could cause thermal fatigue failure due to brittleness. The addition of activated carbon by [17] into Sn-Cu-Ni solder also showed lower IMC thickness with increasing activated carbon content.

There are three main ways in which solder joints can experience shear failure. Mode 1 refers to the ductile fracture mechanism through the penetration across the solder matrix. Bulge fractures with noticeable dimples characterize the resulting cracked surface. As the crack travels through the solder matrix and subsequently the IMC layer in Mode 2, it exemplifies a combined ductile-brittle fracture mechanism. Less cleavage and smaller dimples characterize the fracture surfaces of this mode. Brittle Mode 3 fractures are those that propagate entirely within the interfacial IMC layer. In this mode, surfaces with fractures appear smooth [21]. Mode 1, which is the in-solder failure mode, is preferred, as shown in Table 1. This type of failure within the solder matrix is advantageous because it provides protection for electronic components in electronic packaging and is readily repairable via solder joint reflow processes. Conversely, Mode 2, the IMC failure mode, is undesirable because electronic components soldered onto the IMC layer are vulnerable to the damaging effects of fracturing the layer.

Table 1. Fracture failure modes.

Failure Mode	Conditions
Mode 1 – In Solder Region	Desirable
Mode 2 – Between Solder/IMC Interface	Neutral
Mode 3 – In IMC Interface	Undesirable

Results in Figure 1 are further supported by data in Figure 2 (types of failure modes observed) and Table 2 (percentage of failure modes). The IMC failure mode exhibited the lowest solder strength due to its brittleness, followed by the mixed solder/IMC failure mode and the in-solder failure mode. In-solder failure mode increased with higher activated BC content, particularly in the as-reflowed condition and after 7 days of heat treatment. However, only 33 % of the samples with 1.00 wt.% activated BC exhibited solder mode failure after 14 days aging. In the as-reflowed samples with 1.00 wt.% activated BC, 100 % failed via Mode 1 (in the solder region). No failures via Mode 3 occurred when the as-reflowed samples contained 0.50 wt.% or more of activated BC, and the 7- and 14-day heat-aged samples were free from Mode 3 failures when the activated BC composition was at 0.75 wt.% and above.

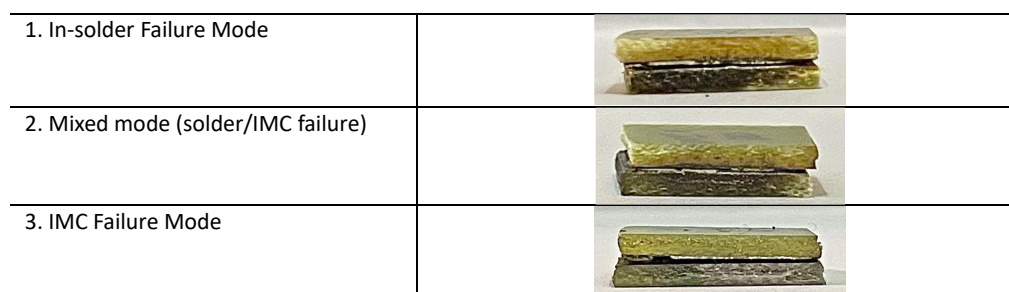


Fig.2. Types of failure modes observed.

Inclusion particles, identified as BC (Figure 3) were observed in dimple areas for majority of the activated BC-containing samples and the dimples were smaller in sizes. Figure 4 showed changes in fracture behaviour when Sn-58Bi was added with varying amounts of activated BC. As-reflowed Sn-58Bi sample had predominantly flat and smooth fracture surface, corresponding to brittle fracture. Besides, intergranular fracture was also observed, consistent with the characteristics of brittle fracture. There was a most notable change to elongated dimple structure with almost no cleavage present when only as low as 0.25wt.% of activated BC was added. Prolonged heat-aging times showed more cleavage. The activated BC serve as supplementary nucleation sites during the solidification of the solder, resulting in a more refined grain structure and, as a result, smaller dimples [22]. This is due to the more uniformly distributed localized stress during fracture. Furthermore, the strong adsorption capability of the activated BC improves interfacial bonding with the solder matrix, which in turn reduces the coalescence of voids and causes smaller dimples when mechanical stress is applied. Fine Bi-precipitates were also present in reinforced samples, indicating that the activated BC particles successfully suppressed segregation of the typically coarse Bi phase. Sizes of these particles increased slightly with aging time due to ripening effects. All pure Sn-58Bi samples exhibited brittle fracture behavior with deep cleavage facets while reinforced samples showed some presence of shallow facets with increasing aging duration. In general, there were less facets in samples containing more activated BC additions. Dimple colonies became more homogeneous when more activated bamboo charcoal was added.

Table 2. Percentage of failure modes for Sn-58Bi reinforced by different weight percentages of activated bamboo charcoal.

0 Day (as-reflowed)					
Failure Mode	SnBi	SnBi + 0.25 wt.% BC	SnBi + 0.50 wt.% BC	SnBi + 0.75 wt.% BC	SnBi + 1.00 wt.% BC
Solder mode	0%	0%	33%	67%	100%
IMC/solder mode	33%	67%	67%	33%	0%
IMC mode	67%	33%	0%	0%	0%

7 days of heat-aging					
Failure Mode	SnBi	SnBi + 0.25 wt.% BC	SnBi + 0.50 wt.% BC	SnBi + 0.75 wt.% BC	SnBi + 1.00 wt.% BC
Solder mode	0%	0%	0%	33%	67%
IMC/solder mode	33%	33%	67%	67%	33%

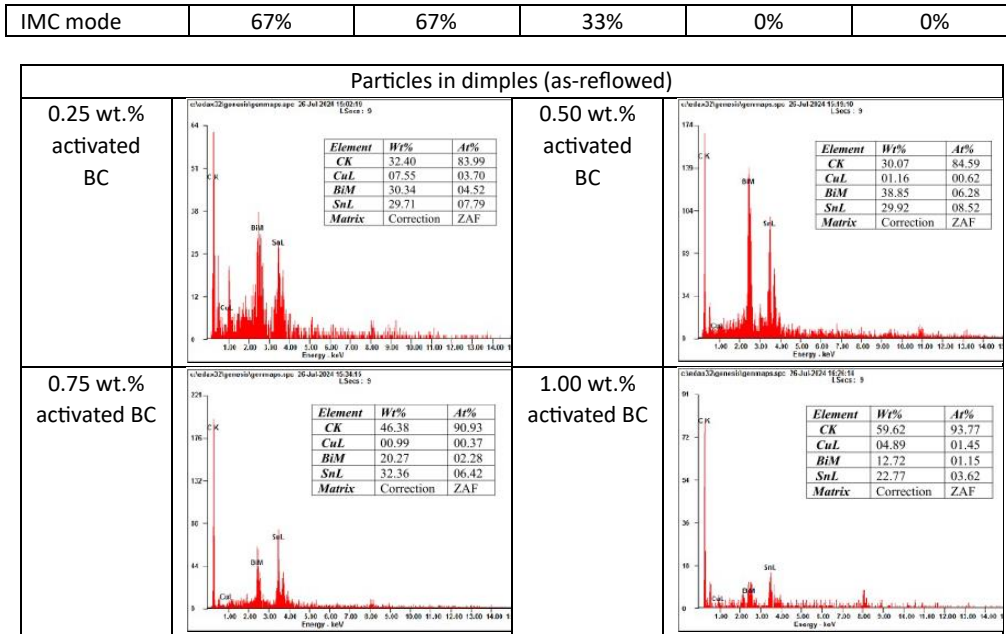
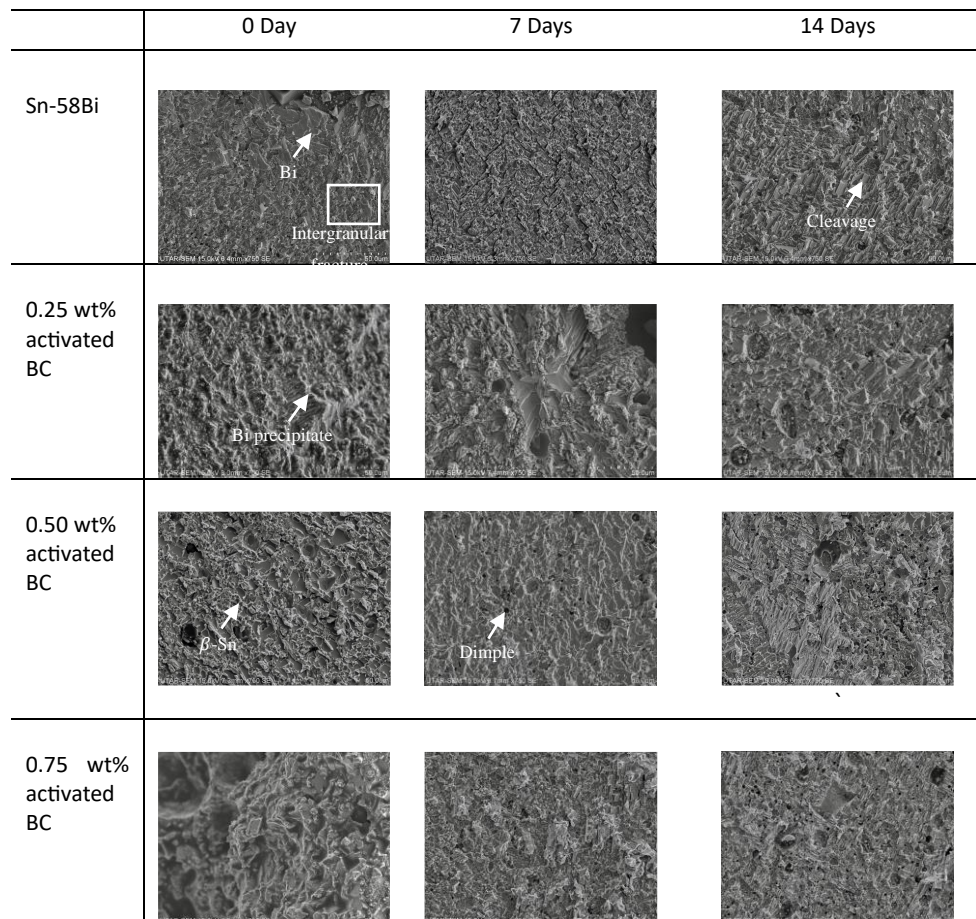


Fig.3. Carbon content in inclusions in dimples (as-reflowed condition).



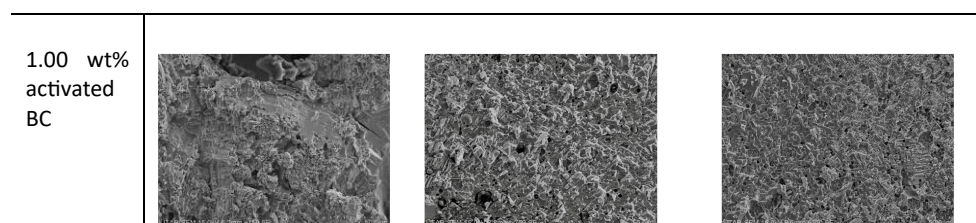


Fig. 4. SEM fractographs for Sn-58Bi with varying activated bamboo charcoal content.

4. Conclusion

In this study, changes in shear strengths of Sn-58Bi alloy containing varying amounts of a plant-based reinforcement, bamboo charcoal and the respective failure modes and fracture behaviour were investigated. The following conclusions can be drawn:

1. The shear strength of Sn-58Bi solder increased with higher activated BC content but decreased with longer heat-treatment durations, with lower degradation rates observed with the addition of BC.
2. The IMC failure mode (Mode 3 – brittle fracture) exhibited the lowest solder strength, followed by the mixed solder/IMC failure mode (Mode 2 - combined ductile-brittle fracture) and the in-solder failure mode (Mode 1 - ductile fracture). Mode 1 failure generally increased with higher activated BC content, while Mode 3 failure increased with longer heat treatment duration.
3. Adding activated BC reinforcement to Sn-58Bi changed its fracture behaviour from brittle to more ductile, transitioning from a flat and smooth surface to elongated dimple structures even at just 0.25 wt.% addition. While prolonged heat-aging increased cleavage presence, more activated BC reduced facet number and dimple size, indicating successful suppression of Bi phase segregation.

Based on the findings of this research, activated bamboo charcoal is a feasible reinforcement to be used to counter the inherent brittleness of Sn-Bi solder as it is not only low in cost but also sustainable and environment-friendly, a step forward in reducing toxic Pb from PV waste.

The authors would like to acknowledge the Centre of Advanced and Sustainable Materials Research, Universiti Tunku Abdul Rahman.